Author Manuscript

Author Manuscript

Author Manuscript

Author Manuscript

HHS Public Access

Author manuscript

Cell Rep. Author manuscript; available in PMC 2022 April 15.

Published in final edited form as:

Cell Rep. 2021 November 02; 37(5): 109916. doi:10.1016/j.celrep.2021.109916.

Epithelial-myeloid exchange of MHC class II constrains immunity and microbiota composition

W. Zac Stephens[1], **Jason L. Kubinak**[2], **Arevik Ghazaryan**[1], **Kaylyn M. Bauer**[1], **Rickesha Bell**[1], **Kate Buhrke**[1], **Tyson R. Chiaro**[1], **Allison M. Weis**[1], **William W. Tang**[1], **Josh K. Monts**[4], **Ray Soto**[1], **H. Atakan Ekiz**[1,3], **Ryan M. O'Connell**[1,*], **June L. Round**[1,5,*]

[1]University of Utah School of Medicine, Department of Pathology, Division of Microbiology and Immunology, Salt Lake City, UT 84112, USA

[2]University of South Carolina School of Medicine, Department of Pathology, Microbiology and Immunology, Columbia, SC 29209, USA

[3]Izmir Institute of Technology, Molecular Biology and Genetics Department, Gulbahce, Izmir 35430, Turkey

[4]University of Utah School of Medicine, Flow Cytometry Core, Health Sciences Center, Salt Lake City, UT 84112, USA

[5]Lead contact

SUMMARY

Intestinal epithelial cells (IECs) have long been understood to express high levels of major histocompatibility complex class II (MHC class II) molecules but are not considered canonical antigen-presenting cells, and the impact of IEC-MHC class II signaling on gut homeostasis remains enigmatic. As IECs serve as the primary barrier between underlying host immune cells, we reasoned that IEC-intrinsic antigen presentation may play a role in responses toward the microbiota. Mice with an IEC-intrinsic deletion of MHC class II ($IEC^{\Delta MHC\ class\ II}$) are healthy but have fewer microbial-bound IgA, regulatory T cells (Tregs), and immune repertoire selection. This was associated with increased interindividual microbiota variation and altered proportions of two taxa in the ileum where MHC class II on IECs is highest. Intestinal mononuclear phagocytes (MNPs) have similar MHC class II transcription but less surface MHC class II and are capable of acquiring MHC class II from IECs. Thus, epithelial-myeloid interactions mediate development of adaptive responses to microbial antigens within the gastrointestinal tract.

This is an open access article under the CC BY-NC-ND license (http://creativecommons.org/licenses/by-nc-nd/4.0/).

*Correspondence: ryan.oconnell@path.utah.edu (R.M.O.), june.round@path.utah.edu (J.L.R.).

AUTHOR CONTRIBUTIONS

J.L.K., W.Z.S., J.L.R., and R.M.O. conceived of the project and experiments. W.Z.S. and J.L.R. wrote the initial manuscript. W.Z.S., J.L.K., A.G., K.M.B., R.B., K.B., T.R.C., A.M.W., W.W.T., J.K.M., and R.S. performed experiments. W.Z.S. and H.A.E. performed or contributed to all bioinformatics processing and analyses. All authors contributed to manuscript review.

DECLARATION OF INTERESTS

The authors declare no competing interests.

SUPPLEMENTAL INFORMATION

Supplemental information can be found online at https://doi.org/10.1016/j.celrep.2021.109916.

Author Manuscript
Author Manuscript
Author Manuscript
Author Manuscript

Graphical abstract

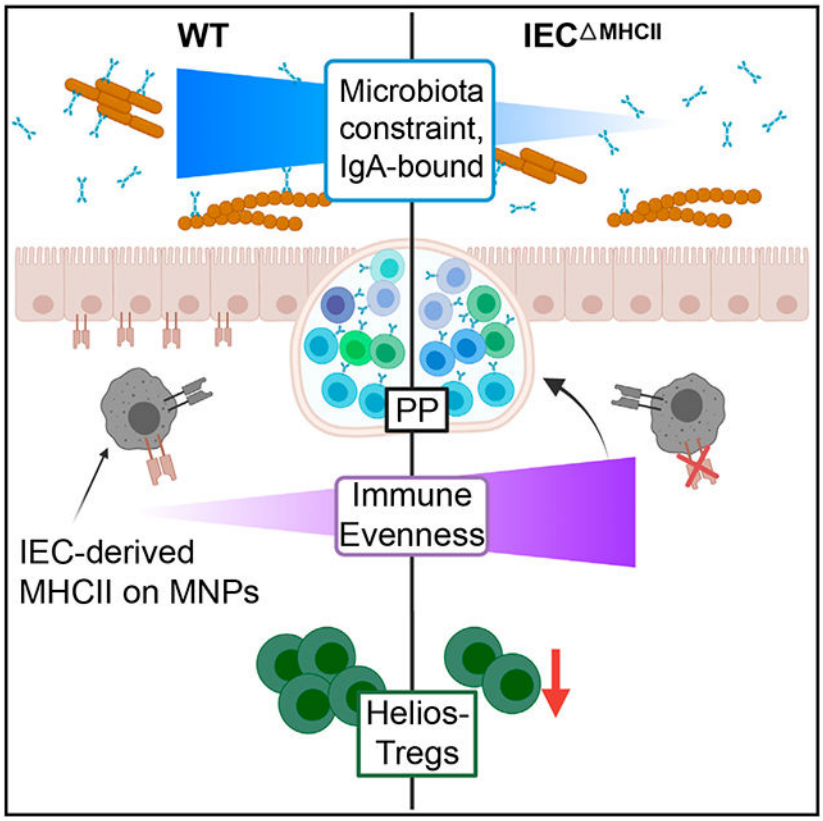

In brief

Recognition of non-self antigens, including gut microbiota, occurs through MHC class II genes found on specific immune cells. MHC class II is also present on intestinal epithelial cells. Stephens et al. show that its loss on epithelia affects microbiota and immune repertoire, and that MHC class II can be transferred from epithelia to underlying immune cells.

INTRODUCTION

Classic major histocompatibility complex class II (MHC class II) molecules play a fundamental role in adaptive immunity by binding and presenting extracellularly derived peptide antigens on the cell surface. These peptide:MHC class II complexes (pMHC class II) then serve as ligands for T cell receptors expressed by $CD4^+$ T cells, and cognate interactions are the first and key step in ensuing effector and memory cell responses. pMHC class II complexes are conventionally expressed by professional antigen-presenting cells (pro-APCs) such as dendritic cells (DCs), macrophages, and B cells, by loading of peptides onto heterodimeric MHC class II proteins (H2-A/E in mice, HLA-DR/DQ/DP in humans) in endolysosomes. H2 proteins present antigens to T cells, inducing effector and memory responses, and thus are integral to the development of adaptive immunity. While the role of MHC class II proteins in adaptive immunity to pathogens has been well studied, the role of MHC class II in coordinating host interactions with the numerous microbes that

Author Manuscript Author Manuscript Author Manuscript Author Manuscript

normally colonize the body (the microbiota) is less understood (Wosen et al., 2018). Most studies have focused on canonical roles of abundant pro-APCs in the lamina propria (LP) and intestinal lymphoid tissue such as mesenteric lymph nodes (mLNs) and Peyer's patches (PPs). However, innate lymphoid cells (ILCs) in the intestine have also been found to express MHC class II molecules and participate in maintaining gut barrier integrity and responses to the gut microbiota (Hepworth et al., 2013). Supporting the role of the MHC class II in shaping the murine microbiota, we have shown that polymorphisms among MHC congenic mice result in distinct gut microbial communities and differential abundance of microbiota-reactive antibodies that impact enteric pathogen susceptibility (Kubinak et al., 2015b). Different MHC alleles in humans have also been demonstrated to impact gut microbiota composition and protect from type 1 diabetes (Silverman et al., 2017). Thus, intestinal MHC class II may play an important role in responding to gut microbial antigens and shaping the microbiota.

In addition to pro-APCs and ILCs, MHC class II surface expression and antigen-presenting capabilities have been reported on other, non-professional APCs from human, mouse, and rat including endothelial cells, mast cells, basophils, eosinophils, and lung and intestinal epithelial cells (IECs) (Bland and Warren, 1986; Hughes et al., 1991; Hershberg et al., 1998; Kambayashi and Laufer, 2014; Dimitriadou et al., 1998; Sokol et al., 2009; Shi et al., 2000; Cunningham et al., 1997). IECs, in particular, express MHC class II proteins with varying reports on expression levels, inducibility, and costimulatory molecule presence from different intestinal locations in mouse and human. In general, small intestinal IECs are reported to express more MHC class II than colonic IECs in the absence of inflammation (Hershberg and Mayer, 2000; Chiba et al., 1988). The currently available data on the functional importance of IEC intrinsic MHC class II expression are scarce, and the results from these limited studies do not always agree. For instance, epithelial-derived MHC class II has been hypothesized to play a role in maintaining intestinal health, as patients with Crohn disease (CD) exhibit differential cellular and tissue distribution of MHC class II proteins (Hundorfean et al., 2007; Bär et al., 2013; Büning et al., 2006). IECs isolated from individuals with inflammatory bowel diseases (IBD) stimulated greater $CD4^+$ T cell proliferation and interferon (IFN)-γ secretion when compared to IECs from healthy patients, indicating that IECs can directly stimulate pathogenic T cell responses (Dotan et al., 2007). However, reduced expression of MHC class II on IECs by deletion of the pIV promoter of the CIITA gene that drives MHC class II expression in IECs was correlated with worsened colitis and increased Th1 cells in a mouse model of colitis with *Helicobacter hepaticus* (Thelemann et al., 2014). A recent publication also deleted MHC class II on mouse IECs and found a slight protection from DSS-induced and T cell transfer colitis but increased susceptibility to *Citrobacter rodentium* infection (Jamwal et al., 2020). In another study, using mice where MHC class II expression was restricted to DCs or IECs, IEC-expressed MHC class II was not required for the development of *Helicobacter bilis*-induced colitis, but rather DC MHC class II was the key mediator of this hyper-inflamed state (Maggio-Price et al., 2013). Furthermore, while the presence of the microbiota or segmented filamentous bacteria (SFB) monoassociation has been reported to induce ileal IEC MHC class II specifically, IEC MHC class II is not required to induce Th17 cell responses against SFB that attach directly to IECs (Koyama et al., 2019; Umesaki et al., 1995; Goto et al., 2014).

Author Manuscript Author Manuscript Author Manuscript Author Manuscript

Thus, while both the microbiota and MHC class II are important contributors to intestinal homeostasis and inflammation, it remains unclear how MHC class II on IECs impacts intestinal homeostasis and microbial composition.

As IECs may interact with many immune cell types in the LP, multiple processes are likely to underlie the role of IECs in the development of mucosal immune responses. IEC-derived MHC class II might influence mucosal immunity through canonical direct interaction with T cells. While *in vivo* evidence is sparse, studies with lung epithelia and many *in vitro* studies using T cells and gut-derived cell lines or organoids provide support for this potential mechanism (Framson et al., 1999; Dotan et al., 2007; Koyama et al., 2019; Rogoz et al., 2015; Westendorf et al., 2009; Biton et al., 2018). While the degree of direct contact of lamina propria T cells with IECs *in vivo* may limit this mechanism, it has been suggested that T cell interaction with $Lgr5^{+}$ IECs can feed back and shape the differentiation of epithelial cells, thereby further impacting mucosal homeostasis (Biton et al., 2018). Besides direct interaction with T cells, intercellular communication of pMHC class II complexes on IECs with mononuclear phagocytic (MNP) cells such as macrophages and DCs might also occur by exosome transfer, trogocytosis, or phagocytosis of dying IECs (efferocytosis) (Cummings et al., 2016). Exosomes are produced in large amounts from IECs, and the IEC-specific glycoprotein A33 has been used to track the appearance of epithelial-derived proteins in DCs in mLNs (Büning et al., 2008; Van Niel et al., 2003). Furthermore, IFN-γ-stimulated IEC cell lines produce more MHC class II^{+} exosomes that are capable of stimulating antigen-specific humoral immune responses (Van Niel et al., 2003). Intercellular communication may also occur through trogocytosis of cell membranes by MNPs known to intimately interact with IECs. Gut-resident tolerogenic DCs, as well as macrophages, can induce or maintain Tregs through retinoic acid or interleukin (IL)-10-dependent signaling mechanisms and can extend dendrites across epithelia to sample lumenal antigens and could potentially acquire portions of IEC cell membranes during this process (Sun et al., 2007; Bain and Schridde, 2018; Murai et al., 2009; Niess et al., 2005). Additionally, an intriguing report suggested that macrophages and DCs themselves exchange membrane proteins in a gap-junction-dependent manner, suggesting a potential mechanism by which resident macrophages may exchange antigens with more mobile DCs that can traffic to mLNs that are major sites of Treg induction (Mazzini et al., 2014). Thus, multiple mechanisms of intercellular communication may transfer microbial antigen-specific signals to underlying immune cells through pMHC class II and influence adaptive immunity to intestinal antigens.

Herein we confirm that the presence of the microbiota induces small intestinal IEC MHC class II expression specifically and report that lack of IEC-derived MHC class II reduces the amount of MHC class II on the surface of intestinal MNPs and results in a reduction of $Helios^{-}$ microbial-responsive Tregs, suggesting that MNPs participate in a network of communication with IECs and Tregs. The loss of MHC class II on IECs results in reduced selection of B cell receptor (BCR) repertoires, increased fecal microbiota variability and ileal expansion, and increased susceptibility to DSS-induced colitis. These results thus demonstrate a role for IEC-derived MHC class II in constraining microbiota composition and inducing tolerogenic responses against it.

Author Manuscript Author Manuscript Author Manuscript Author Manuscript

RESULTS

MHC class II is differentially expressed within intestinal epithelia and induced by the microbiota

Given its proximity to gut microbial antigens, as well as its established role in mucosal immunity, we hypothesized that epithelial cell-derived MHC class II expression may play a key role in the development of immune responses to the microbiota. To determine where epithelial MHC class II expression is likely to exert its greatest effect, we first characterized the expression of surface MHC class II using an antibody against the H2-A heterodimer on live, $CD45^{-}$, $EpCAM^{+}$ IECs by flow cytometry under homeostatic conditions in wild-type (WT) C57BL/6 mice. Cell-surface H2-A was found on the highest proportion of cells in the small intestine but consistently expressed throughout the small intestine and colon, and the highest per cell expression was within the ileum (Figures 1A, 1B, and S1). This is consistent with a recent publication and suggests that the pattern of MHC class II expression along the intestinal tract is not dependent on different microbiota between facilities (Koyama et al., 2019). Immunohistochemistry of ileal sections showed high levels of punctate H2-A in intracellular vesicles located apically but also showed less intense but diffuse surface staining of H2-A throughout the basolateral surface of IECs (Figure 1C). Previous reports have shown that germ-free C57BL/6 and BALB/c mice have reduced or absent MHC class II on IECs (Umesaki et al., 1995; Koyama et al., 2019). To determine whether the induction of MHC class II on IECs by the microbiota is a general feature of the murine intestine and not a strain-specific effect, we similarly characterized cell-surface H2-A on IECs from age-matched germ-free and SPF Swiss-Webster mice. Again, ileal IECs expressed much higher levels of H2-A than colonic cells in this experiment; however, ileal H2-A was greatly reduced in the absence of the microbiota while the low-level expression of colonic H2-A was unaffected (Figures 1D-1F). These data indicate that the microbiota influences expression of H2-A within IECs of the small but not large intestine.

IEC-intrinsic MHC class II controls variability of the microbiota

We, and others, have previously shown that MHC class II haplotype can influence the composition of the microbiota (Kubinak et al., 2015b; Bolnick et al., 2014; Silverman et al., 2017; Khan et al., 2019; Melo-Gonzalez et al., 2019). Given this, and the proximity of abundant MHC class II expression by IECs to the microbiota, we hypothesized that knocking out MHC class II on IECs specifically would result in significant shifts to the structure and composition of the gut microbiota. We therefore crossed *H2-Ab1* floxed mice with an IEC-specific Cre driver (*Villin*:Cre)(Hashimoto et al., 2002; Madison et al., 2002). These mice had near-complete loss of surface H2-A on their IECs, and we refer to these mice hereafter as $IEC^{\Delta MHCII}$ and used Cre-negative *H2-Ab1* floxed littermates as WT controls for all comparisons (Figures 2A and S2A). To understand whether a lack of IEC MHC class II expression altered their transcriptional profile, we performed bulk RNA-seq of sort-purified IECs from the ileums of WT and $IEC^{\Delta MHCII}$ mice. This analysis confirmed the knockout of *H2-Ab1* but detected no other significantly differentially expressed genes, indicating that loss of MHC class II within IECs had little effect on the function of these cells (Figure 2B). We next sought to address the potential of an IEC-intrinsic defect not observed from sorted IEC transcriptomes. Intestinal barrier function

Author Manuscript Author Manuscript Author Manuscript Author Manuscript

was assessed by gavaging mice with FITC-dextran and assaying the amount in the blood. No difference in the intestinal permeability of IEC$^{\Delta MHCII}$ mice was detected among 3 independent experiments (Figure S2B). Additionally, we assessed the transcription of 5 genes involved in tight junction formation (*Tjp1, Tjp2, Tjp3, Cldn7*, and *Cldn2*) by qRT-PCR of intact ileal tissue. We found no difference between WT and IEC$^{\Delta MHCII}$ mice of *Tjp2, Tjp3, Cldn7*, and *Cldn2* and just a 2-fold increase in the transcription of *Tjp* 1 (Figure S2C). We also examined the number of Caspase3^{+} cells per villi or Ki67^{+} cells per crypt in immunohistochemical-stained intestinal sections to determine whether apoptosis or cell-cycle were impacted by deletion of IEC MHC class II. Again, we found no significant differences in the number of Ki67^{+} or Caspase3^{+} (Figures S2D and S2E). Taken together, our data suggest that loss of *H2-Ab1* within IECs does not alter their intrinsic function.

We next assessed microbiota composition by 16S rRNA gene sequencing of feces from WT and IEC$^{\Delta MHCII}$ siblings separately housed by genotype since weaning. We detected few differences in these animals, with no significant differences in alpha diversity metrics and 2 ASVs (Amplicon Sequence Variants) from the abundant S24-7 family of Bacteroidales reduced in the feces (ANCOM, $W = 264$ and *253* among 267 ASVs) (Figure S3A). The IEC$^{\Delta MHCII}$ microbiota clustered significantly different from WT by the non-phylogenetic abundance-weighted Bray-Curtis distance and both unweighted metrics but not by the phylogenetic weighted-UniFrac distance, and the distance between IEC$^{\Delta MHCII}$ mice was greater than the distances between WT mice, suggesting these small differences are mainly driven by variability in the microbiota of IEC$^{\Delta MHCII}$ mice at the level of ASVs (Figures 2C and 2D; Table S1; Figure S3B). Differences between groups when mice are housed together can be driven by changes in one or a few animals due to coprophagy, in addition to ecological drift between cages. Therefore, we also assessed the fecal microbiota each week after weaning for 4 weeks in WT and IEC$^{\Delta MHCII}$ offspring individually housed after weaning at 3 weeks of age. We did not detect any significantly different taxa between genotypes, although we again found significantly increased dissimilarity among IEC$^{\Delta MHCII}$ animals' microbiota at 4 and 7 weeks of age (Figure 2E). MHC class II is induced in the ileum by the presence of the microbiota (Figures 1D and 1E). Therefore, we next examined the composition of the ileal microbiota in animals separated by genotype since weaning or continuously cohoused. In separately housed animals, genotype significantly separated the microbiota of IEC$^{\Delta MHCII}$ with both phylogenetic and non-phylogenetic beta diversity metrics but was not significant when animals were cohoused (Table S1; Figure 2F). In separately housed animals, 4 ASVs were detected as different in the ileum between genotypes by ANCOM analysis, including 2 belonging to the S24-7 family (ANCOM, $W =$ 113 and 112 among 121 ASVs) that were increased this time in IEC$^{\Delta MHCII}$ ileal microbiota and 2 ASVs classified as *Bifidobacterium pseudolongum* (ANCOM, $W = 119$ for both) that were decreased. These differences were again not detected in cohoused animals (Figure 2G). Adonis analysis of Bray-Curtis dissimilarities showed that both cage and genotype accounted for a significant proportion of the microbiota variation (Figure 2F). Interestingly, despite no differences observed in the fecal microbiota, the ileal microbiota of IEC$^{\Delta MHCII}$ animals exhibited an increase in the Shannon diversity index driven by a significant increase in the number of observed ASVs detected in the ileum (Figure 2H). Overall, while drastic changes in the fecal microbiota were not present within animals that lack IEC-intrinsic MHC

Author Manuscript Author Manuscript Author Manuscript Author Manuscript

class II, the ileal microbiota composition is affected IEC MHC class II. Our data suggest that IEC-intrinsic MHC class II is responsible for reducing variation in the composition of the fecal microbiota between individuals and controls expansion of the ileal microbiota.

Lack of IEC-derived MHC class II results in reduced microbiota-induced Tregs and increased susceptibility to colitis

Given that MHC class II is central to the generation of $CD4^+$ T cell responses, we profiled the immune state within the intestine of $IEC^{\Delta MHCII}$ mice. As MHC class II expression is highest on IECs of the small intestine, we focused on immune responses associated with this site, including mLN, PP, and siLP (small intestinal lamina propria). No differences were detected in the proportion of inflammatory Th17 or Th1 cells (Figures S3C and S3D). Because germinal center reactions are known to be important for constraining microbiota composition, we additionally assessed follicular T cell (Tfh), T follicular regulatory (Tfr), and germinal center B (GCB) cells but found no differences in the proportions or abundances of these cells in PP or mLNs (Figures S3E-S3G) (Kawamoto et al., 2014). We further assessed the recruitment of antigen-specific T cells into germinal centers by adoptively transferring CD45.1 marked OT-II T cells into sublethally irradiated WT and $IEC^{\Delta MHCII}$ mice and then provided OVA antigen in drinking water *ad libitum* for 3 weeks. Again, we could not detect a difference in the amount of Tfh or Tfr OT-II cells in either PP or mLNs (Figure S3H).

Tregs in the gut have been categorized by the expression of multiple surface markers. In addition to Foxp3 marking Tregs, the lack of expression of the transcription factor, Helios, has been suggested to identify a distinct population of Tregs within the gut and lack of Helios is associated with microbiota-induced Tregs (Thornton et al., 2010; Lathrop et al., 2011). We detected a consistently decreased proportion of $Helios^-$ Tregs among 3 experiments in the siLP, PP, and mLN of $IEC^{\Delta MHCII}$ mice with the most significant decrease being present within the PP (Figures 3A and 3B; Table S2). Thus, MHC class II on IECs appears to be particularly important for maintaining microbiota-induced Tregs.

Tregs are critical for maintaining tolerance to the microbiota and loss of Treg function results in colitis (Atarashi et al., 2013; Furusawa et al., 2013; Boehm et al., 2012). We therefore hypothesized that $IEC^{\Delta MHCII}$ with reduced Tregs would have an increased susceptibility to develop colitis. We treated mice for 6 days with an acute model of DSS-induced colitis and found that, while $IEC^{\Delta MHCII}$ mice did not differ in weight loss or colon length, these animals presented with significantly enhanced pathology in the colon (Figures 3C-3F). Although DSS-colitis is a model of colonic inflammation and IEC-MHC class II is mainly expressed in small intestinal IECs, low-level colon IEC MHC class II was observed under homeostatic conditions (Figures 1A and 1B), and mouse colonocytes can induce MHC class II expression in a T cell transfer model of colitis (Jamwal et al., 2020). Additionally, Tregs can traffic between LP and mLNs that connect both tissues and are a major site of Treg induction (Pabst, 2013). $ROR\gamma t^+Helios^-$ Tregs have been demonstrated to be important for the maintenance of intestinal homeostasis (Britton et al., 2019). These Tregs are particularly abundant within the colon but are also present in mLNs, PPs, and the siLP (Sefik et al., 2015). While we did not see differences within

Author Manuscript Author Manuscript Author Manuscript Author Manuscript

RORγt$^+$Helios$^-$ Tregs (CD3$^+$CD4$^+$Foxp3$^+$) during the steady state, RORγt$^+$Helios$^-$ Tregs were significantly reduced in the mLNs during DSS colitis (Figure 3G). RNA sequencing (RNA-seq) on ileal tissue from DSS-treated mice again showed modest changes to the overall transcriptome, despite including IECs as well as all underlying LP cells in this experiment, with no significantly differentially expressed genes after controlling for multiple hypothesis testing (Figure S4A). Additionally, we could not detect any difference in the ileal microbiota composition by any diversity metrics or taxonomic composition analysis in DSS-treated animals (Table S1). These data suggest that a lack of induction of Helios$^-$ Tregs may result in hyperresponsiveness to microbial antigens leading to increased intestinal damage in IEC$^{\Delta MHCII}$ mice during colitis.

IEC intrinsic MHC class II expression influences surface MHC class II levels on macrophages and monocytes

A few studies have demonstrated that IECs can directly stimulate T cell responses *in vitro*, and these interactions may drive expansion of Tregs preferentially (Westendorf et al., 2009; Framson et al., 1999; Dotan et al., 2007). However, a recent study utilizing intra-vital microscopy to map the location of intra-epithelial CD4$^+$ T cells and Tregs demonstrated that the vast majority of Foxp3$^+$ Tregs within the intestine are restricted to the lamina propria and not found closely associated with the epithelia (Sujino et al., 2016). Additionally, DCs conditioned in the presence of IECs then co-cultured with T cells can induce Tregs (Iliev et al., 2009). These studies suggest that direct IEC MHC class II-mediated antigen presentation to Tregs is not the only pathway by which IEC MHC class II can impact Tregs. We identify reductions in Treg populations in areas of follicle formation such as PP and mLN, where proAPCs reside to stimulate T cell responses. Mononuclear phagocyte (MNP) populations, including macrophages and DCs, have well-established roles in maintaining gut homeostasis particularly by inducing microbiota-responsive Tregs in the LP as well as in the mLNs and also play important roles in maintaining epithelial barrier integrity (Bain and Schridde, 2018; Joeris et al., 2017; Sun et al., 2007). Moreover, these cell types are known to be in contact with intestinal epithelial cells (Niess et al., 2005). Given the reduced Helios$^-$ Tregs in IEC$^{\Delta MHCII}$ mice, we compared MNP populations between mutant and WT mice under steady-state conditions. Initially, we used a broad gating strategy (CD45$^+$CD11b$^+$CD11c$^+$MHC class II$^+$CD103$^-$) along the length of the intestine to determine whether loss of IEC intrinsic MHC class II affected MNPs. While there was no difference in the proportion of these cells in the colon or mLN, there was a decrease of these cells in the PP and a particularly striking reduction in the siLP of mice that lacked MHC class II within epithelia (Figure 4A), suggesting that IEC intrinsic MHC class II can influence surface MHC class II levels on MNPs.

Next, to better define the various myeloid populations, we defined CD45$^+$,Lin$^-$,CD11b$^+$CD11c$^+$CX3CR1$^+$ monocyte-macrophages similar to the “P1–P4 waterfall” model of differentiation, and we defined DCs as CX3CR1$^-$CD103$^+$ from within the CD11b$^+$CD11c$^+$ subsets (Joeris et al., 2017; De Calisto et al., 2012) (Figure 4B). We observed a differential representation of the proportion of MNPs, including an increase in P1 monocytes in the siLP and mLN of IEC$^{\Delta MHCII}$ mice along with reduced proportions of P2 transitioning monocytes in the mLN and reduced P3/4 macrophages in the siLP

Author Manuscript Author Manuscript Author Manuscript Author Manuscript

and mLN (Figure 4C). Surface MHC class II is frequently used as a primary marker of MNP populations, while in the waterfall model the amount of surface MHC class II (H2-A here) defines differentiating (P2) or differentiated macrophages (P3/4). We consistently observed small reductions in the amount of surface H2-A on these H2-A$^+$ P2 and P3/4 cell subsets, with significant decreases in the mLNs where these cell types are rarer (Figure 4D). While we observed no difference in the proportion of DCs with these markers, we did find a decrease in the proportion of DCs that were H2-A$^+$ at all sites, and a decreased abundance of surface H2-A on DCs in the siLP and mLN (Figures 4E and 4D). Because levels of the integrins that comprise CD11c can vary among these cell populations, we also examined the P1–4 populations within the Lin-, CD11b$^+$CD11c$^-$CX3CR1$^+$ cells (Joeris et al., 2017) (Figures S5A and S5D). These CD11c$^-$ cells' H2-A patterns were generally in agreement with the CD11c$^+$ populations (though we did not detect sufficient CD11c$^-$ P3/P4 macrophage subsets in the PP), with strong decreases in the proportion of P3/P4 macrophages and H2-A MFI on siLP macrophages (Figures 4F, S4B, and S4C). These data suggest that an absence of MHC class II on IECs can impact the differentiation, activation, and/or function of underlying myeloid cells. To determine whether MNPs from IEC$^{\Delta MHCII}$ were less activated than WT MNPs, we assessed intracellular versus surface H2-A among H2-A$^+$ DCs and P3/4 macrophages, and the abundance of the CD80 costimulatory molecule. We could not detect differences in the percentage of CD80$^+$ cells or the MFI of CD80 in the siLP or mLNs of IEC$^{\Delta MHCII}$ mice (Figures S4D and S4E). While the percentage of surface H2-A$^+$ cells was again reduced in IEC$^{\Delta MHCII}$ mice, among H2-A$^+$ cells we generally did not detect a difference in the ratio of surface and intracellular H2-A indicating there was no difference in the activation state of these cells, except for CD11c$^+$ macrophages in the mLNs that exhibited a significant reduction (Figure S4F). The reduced H2-A on MNPs may reflect reduced extracellular acquisition of H2-A in IEC$^{-\Delta}$MHC^{II} mice.

MHC class II on IECs constrains immune responses to intestinal microbes

Since these results suggest that loss of IEC MHC class II was able to impact cellular phenotypes beyond just CD4$^+$ T cells, single-cell sequencing (scRNA-seq) was used to better assess the potential global immune effects of loss of IEC MHC class II. scRNA-seq libraries were prepared with the 10X genomics platform from MACS-sorted CD45$^+$ cells of the siLP and PP and repertoires of B cell receptors (BCRs) were obtained from the same cells. There were no dramatic differences in the representation of various cell types based on their transcriptional profile between the WT and IEC$^{\Delta MHCII}$ strains (Figures S5A and S5B). However, we did observe a difference in the BCR repertoires in the PPs. IEC$^{\Delta MHCII}$ mice had a more even distribution of Ig clonotypes than WT mice, which were dominated by a single clone and had fewer clones present at an even sampling depth (Figures 5A and 5B). These data are reflective of stronger clonal selection in WT mice, while loss of IEC MHC class II leads to more permissive expansion of B cell clones. We could not detect a significant difference in the number of mutations per clonotype in IgA, IgG1, and IgG2b antibody isotypes in PP, consistent with a report of sorted IgA plasma cells from these animals (Figure S5C) (Jamwal et al., 2020). In addition to having more Ig clonotypes, IEC$^{\Delta MHCII}$ BCR isotype frequencies were also skewed, with a decreased proportion of clonotypes carrying IGHA chains and increased proportion of IGHD and IGHM (Figure 5C), suggesting fewer distinct class-switched IgA producing B cells are

Author Manuscript Author Manuscript Author Manuscript Author Manuscript

present in the absence of IEC MHC class II. Quantification of IgA and IgG levels by ELISA from fecal supernatants revealed an increased total amount of both isotypes from mutant mice, however, less IgA-bound gut bacteria in $IEC^{\Delta MHCII}$ mice (Figures 5D-5F and S6). Consistent with a previously shown role for Tregs in IgA selection, the difference in IgA production between WT and mutant mice is lost when $IEC^{\Delta MHCII}$ were crossed onto a genetic background that results in the loss of conventional $CD4^+$ T cells ($TCR\beta^{-/-}$) (Kawamoto et al., 2014; Cong et al., 2009) (Figure 5G). Taken together these data show that MHC class II on IECs influences T cell-dependent antibody responses and suggest the more evenly distributed immune repertoires in $IEC^{\Delta MHCII}$ mice have less high-affinity IgA toward intestinal microbes.

MNPs can acquire MHC class II from IECs

From the scRNA-seq profiling, differences within the transcriptional profiles of MNPs between WT and $IEC^{\Delta MHCII}$ mice were not detected, including differences in the transcription of *H2-Ab1*. This observation indicates that leaky Cre expression in MNPs was not inadvertently impacting endogenous MHC class II function in these cells, thus validating that the observed decrease in protein expression of H2-A on MNPs is not an artifact of the genetic manipulation (Figures 6A and S5E). Since decreases of MHC class II on MNPs are seen at the protein but not the transcript level, and siLP MNPs do not appear to be differentially activated, these data support the possibility that MNPs acquire H2-A protein from IECs.

To test the possibility that MNPs acquire MHC class II proteins from IECs, we devised an experimental *in vitro* association setup using MHC class II-expressing IECs and bone-marrow cells isolated from *H2-Ab1*$^{-/-}$ mice either skewed toward macrophages or DCs. MODEK cells (mouse duodenum derived) were used as IECs and express a distinct MHC haplotype ($H2\text{-}A^k$, recognizable by an antibody that does not cross-react with the $H2\text{-}A^b$ from C57BL/6 mice), thus ensuring we could confidently distinguish IEC-derived $H2\text{-}A^k$. In addition, we either placed these bone-marrow-derived macrophages (BMMs) or DCs (BMDCs) in direct contact with MODEK cells or a transwell system to determine whether the transfer of H2-A was cell-contact dependent. MODEK cells were stimulated to induce MHC class II expression with IFN-γ and Pam3CSK4, and then MNPs were added and assayed for $H2\text{-}A^k$. IEC-derived $H2\text{-}A^k$ was detected on the *H2-Ab1*$^{-/-}$ BMMs and somewhat on BMDCs; however, $H2\text{-}A^k$ was detected more frequently on BMMs than BMDCs when cells were both in contact or in a transwell setup (Figure 6B). The total amount of MHC class II delivered, as indicated by the MFI of MHC class II, was much higher in BMMs that were in contact with IECs than in transwells, although because we normalized MODEK cells to the surface area in these different conditions, fewer MODEK cells are present in the transwell system (Figure 6B). These data suggest that both cell-contact-dependent mechanisms, such as trogocytosis, and secreted molecules, such as exosomes, are capable of delivering MHC class II molecules from IECs to myeloid cells.

As bone-marrow-derived cells are functionally distinct from MNPs within the gut, MNPs were also directly isolated from the siLP and incubated with MODEK cells. Fluorescence-activated cell-sorted (FACS) monocytes ($Dump^-CD45^+Ly6C^{hi}$) and

Author Manuscript Author Manuscript Author Manuscript Author Manuscript

macrophages (Dump^{-}CD45^{+}Ly6C^{-}CX3CR1^{+} CD64^{+}) from siLP or mLNs of *H2Ab1*$^{-/-}$ mice were incubated with MODEK cells (which had been stimulated for 2 days under MHC class II stimulating conditions as above) for 1 day. A significant amount of IEC-derived H2-A^{k} was detected on both *H2Ab1*$^{-/-}$ monocyte and macrophages isolated from siLP, with siLP Ly6C^{hi} monocytes exhibiting the greatest apparent acquisition of H2-A from MODEK cells (Figure 6C). Together these data demonstrate that intestinal MNPs can acquire surface MHC class II from IECs.

To test whether MNPs with reduced IEC-derived MHC class II had different Treg inducing activity, we sorted MNPs from PPs of WT and IEC$^{\Delta MHCII}$ mice with CD45^{+}CD3^{-}CD19^{-}CD11b^{+}CD11c^{+}CD103^{-} markers, pulsed them with OVA peptide, and incubated them with CFSE-labeled splenic OT-II CD4^{+} T cells. These MNPs could contain macrophages and some cDC subsets based on this sort strategy but was necessary to acquire enough cells to coculture with OT-II T cells (Cerovic et al., 2013). MNPs isolated from IEC$^{\Delta MHCII}$ mice stimulated more T cell proliferation than WT MNPs, but fewer of the proliferated cells were Foxp3^{+} compared to MNPs isolated from WT mice (Figure 6D). Thus, MNPs with reduced surface MHC class II isolated from animals that lack IEC-derived MHC class II have a decreased capacity to suppress proliferation and support Treg induction or maintenance.

We next sought to test the ability of MNPs to interact with and acquire H2-A from IECs *in vivo*. First, we used the mT/mG genetic mouse model to determine whether we could detect labeled MNPs that had acquired membrane fragments from labeled IECs. In this model, membrane targeted tandem dimer tomato fluorescent protein (mT) is constitutively expressed by all cells, and when a Cre-mediated excision event occurs the cells begin to express membrane targeted GFP (mG) (Muzumdar et al., 2007). We therefore crossed these mT/mG mice to mice carrying the same Villin:Cre driver we used to knockout *H2-Ab1* from the intestinal epithelium, such that GFP signal would be expected to only be present on IEC membranes and then assayed siLP macrophages and DCs for GFP. A small but significant fraction of both CD11c^{+} and CD11c^{-} macrophages appeared to acquire membrane fragments from IECs as seen by the proportion of mT^{+}mG^{+} cells. A considerably higher proportion of DCs were mT^{+}mG^{+} (Figure 7a). imaging flow cytometry of the mT^{+}mG^{+} MHC class II^{+} cells from the siLP showed that the GFP was typically found in a punctate pattern on these cells, further supporting that this was likely extracellularly acquired membrane GFP (Figure 7B). These assays support that MNPs are capable of acquiring IEC membrane fragments.

We next sought to specifically determine whether underlying MNPs in the siLP acquired MHC class II molecules from the iECs *in vivo* by transferring bone-marrow cells with a distinct MHC class II from the MHC class II allele on C57BL/6 mice. We used our WT and IEC$^{\Delta MHCII}$ mice in the TCR$\beta^{-/-}$ background (H2-A^{b} allele) as recipient mice and NSG-Ab DR4 mice as donors. These humanized donor mice were developed to study graft-versus-host disease and, in addition to being T cell deficient due to the SCID mutation and IL2r$\gamma^{-/-}$, carry a transgenic human MHC class II allele (HLA-DR4) and are mouse *H2-Ab1*$^{-/-}$ (Covassin et al., 2011). This allowed us to accurately distinguish 2 different MHC class II proteins (endogenous, donor cell derived, and host derived) on the same cells (Figure

Author Manuscript Author Manuscript Author Manuscript Author Manuscript

7C). Following lethal irradiation, we transferred 3.8×10^6 bone-marrow cells into host mice and allowed the cells to engraft for 8 weeks before assessing the amount of host-derived H2-A^b on siLP resident MNPs. After this time frame post-transfer, we could not detect sufficient engraftment of HLA-DR^+ donor cells in the spleen or mLN but found abundant $CD11c^-$ macrophages in the siLP. Interestingly, donor $CD11c^+$ macrophages and donor DCs in the siLP were not abundant enough to accurately assay (Figure S7). However, we detected a significant decrease in the percentage of HLA-DR^+, $CD11c^-$ donor macrophages in the siLP that also carried host H2-A^b (Figure 7D). While this does not exclude the possibility of transfer to other cell types, these *in vivo* data demonstrate that, at least, $CD11c^-$ ileal macrophages can specifically acquire IEC-derived MHC class II.

DISCUSSION

Abundant IEC-expressed MHC class II has been reported for decades, yet the exact roles of this non-canonical expression for immunity have been difficult to determine. Indeed, lack of MHC class II on IECs results in healthy mice under homeostatic conditions despite the high expression level on these cells. Here, we reported an unexpected transfer of MHC class II molecules between IECs and MNPs. Lack of IEC MHC class II resulted in decreased microbiota-induced Tregs, increased microbiota variability and altered ileal composition, and we have validated that ileal IEC MHC class II is inducible by the microbiota. These data implicate a role for IEC-derived MHC class II in a network of MHC class II molecule exchange among intestinal immune sites that serve to constrain intestinal immune responses and gut microbiota composition.

Intestinal lamina propria MNPs can reside adjacent to IECs and may extend processes in between IECs (Niess et al., 2005). Among MNPs, DCs and macrophages participate in an exchange of pMHC class II that is gap junction dependent and facilitates the development of oral tolerance (Mazzini et al., 2014). Both cell types can play a role in Treg induction, although more mobile DCs are particularly effective Treg inducers at more distal sites such as mLNs and can be conditioned by small intestinal IEC-derived factors (Iliev et al., 2009). The data presented here cannot exclude the possibility that direct IEC-T cell interaction also contributes to inducing peripheral Tregs, and the lack of transcriptomic differences suggests that DCs are not differentially conditioned by IECs from $IEC^{\Delta MHCII}$ mice. Here, we extend the network of MHC class II molecule intercellular exchange to include IECs and the abundant MHC class II found on them. While we cannot exclude the possibility that all MNPs are capable of acquiring IEC MHC class II, our data point to the importance of macrophages, in particular, in acquiring MHC class II from IECs. These APCs have endogenous MHC class II expression of their own and how, or whether, extracellularly acquired pMHC class II might be differentiated is an interesting future question. However, as the transition from monocyte to macrophage is well established to involve the upregulation of surface MHC class II and our data pointed to $Ly6C^+$ monocytes as particularly effective at acquiring IEC-derived H2-A, while no differences were found in the activation status of macrophages, it raises the intriguing possibility that extracellular acquisition of MHC class II in the small intestine may play a role in monocyte-derived macrophage development at this site. Until recently, it was believed that all intestinal macrophages were derived of bone-marrow monocytes, but recent studies have shown

Author Manuscript Author Manuscript Author Manuscript Author Manuscript

that intestinal tissue resident macrophages are also generated from gut-resident embryonic precursors found in all layers of the ileum (De Schepper et al., 2018; Shaw et al.,2018). While we did not distinguish between these and monocyte-derived macrophages, it will be of immediate interest to determine whether these or other macrophages subsets are most efficient at acquiring IEC-derived MHC class II.

Several potential mechanisms may facilitate exchange of MHC class II among cells, but how long antigens loaded onto MHC class II remain intact among this network, and whether these are differentiated from cell intrinsic pMHC class II, is unknown. Exosome uptake, efferocytosis, and trogocytosis have all been postulated as mechanisms of intercellular exchange of membrane and proteins from IECs. All mechanisms likely occur in some context. Our data support that both cell-contact-dependent and contact-independent mechanisms are relevant. Exosomes are produced abundantly from IECs, can contain surface MHC class II, and are capable of inducing peripheral tolerance earning them the moniker “tolerosomes” (Van Niel et al., 2003; Östman et al., 2005; Karlsson et al., 2001). It may be that IEC-produced exosomes are taken up by a specific subset of MNPs and induce tolerance by direct TCR interaction in the absence of costimulatory molecules. Efferocytosis is a dynamic process that may have inflammatory or anti-inflammatory effects and under normal circumstances results in production of anti-inflammatory cytokines, so is an attractive potential mechanism by which the rapidly proliferating MHC-class-II-containing IECs could impact development of tolerance dependent on macrophages. However, efferocytosis likely results in more general tolerance due to IL-10, IL-13, and transforming growth factor (TGF)-β from M2-like macrophages, rather than antigen-specific tolerance as phagocytosed cells are degraded *en masse* and differential recognition of extracellular-acquired pMHC class II would seemingly be required to prevent its degradation in the lysosome. During trogocytosis, membrane patches and proteins are transferred between cells potentially allowing the recycling of extracellular pMHC class II to be regulated by ubiquitination as for endogenous pMHC class II in APCs (Cho et al., 2015). Interestingly, basophils have already been shown to acquire pMHC class II from DCs through trogocytosis, which explained the presence of surface MHC class II on basophils and their Th2-stimulating capabilities despite little corresponding transcription of MHC class II genes (Miyake et al., 2017). Similarly, ILC2s express MHC class II genes but also have been reported to acquire surface MHC class II from proAPCs through trogocytosis (Oliphant et al., 2014). It is through the mechanism of trogocytosis that closely interacting monocytes or macrophages appear most likely to acquire pMHC class II from IECs and participate in the development of adaptive immune responses to intestinal antigens.

Tregs and secreted IgA play important roles in shaping gut microbial communities, which normally exhibit high interpersonal variation reflective of individualized adaptive immune responses as well as stochastic assembly factors. Due to the stochasticity inherent in the encounter of commensal microbial antigens, perturbations to adaptive immune responses alone, which respond only to antigens encountered, may not necessarily be predicted to result in distinct taxonomic groups being differentially represented consistently among individuals given the normal intra- and inter-individual variation in microbiomes. Rather, adaptive immune defects should be predicted to primarily reflect a lack of shaping or constraint of communities due to reduced immune repertoire selection. Indeed, we observe

Author Manuscript Author Manuscript Author Manuscript Author Manuscript

reduced constraining of the immune repertoire and microbiota when MHC class II is removed from IECs and, in accordance, previously reported that microbiota variance was one of the most distinguishing characteristics between microbiota of mice with different MHC class II haplotypes (Kubinak et al., 2015b). Because there is considerable strain-level variation within microbiomes which reflects antigenic variation, it is perhaps not surprising that we could not detect significant differences among taxonomic groups but could detect a few significantly different ASVs. The reduced microbiota-responsive immune constraint that is exhibited without MHC class II on IECs resulted in increased intestinal pathology in a DSS-induced colitis model, highlighting how reduced immune constraint can lead to hyperresponsiveness to microbiome antigens. Thus, MHC class II on IECs is important for constraining adaptive responses to gut microbial antigens and maintaining intestinal homeostasis.

Limitations of study

Challenges in examining origins of H2-A on MNPs and its role in colitis

—Experiments to examine the cellular origins of proteins that are exchanged between cell types and endogenously transcribed in these cells require differential identification. These experiments are especially challenging when these proteins are involved in histocompatibility such as those in the MHC class II. While we detected transfer of different H2-A haplotypes in the siLP of a T cell-deficient mouse background (Figures 7C and 7D), T cells are involved in inducing IEC H2-A via IFN-γ so this T cell-deficient model may not faithfully recapitulate the natural location and signals in the LP but was useful in avoiding GVHD (Koyama et al., 2019). Future studies could build upon this model by carefully determining the timing after donor cell engraftment needed to detect transfer and not induce disease, removing only donor alloreactive T cells, and by microscopically examining the location of host and donor MNPs relative to IECs in intact tissue. The use of MNP lineage markers that are independent of activation state would help delineate intercellular exchange of commonly used MNP cell markers such as H2-A. While H2-A (MHC class II) is typically used as an early-gate marker of these cell types, throughout this report we assess its cell-surface abundance after using other markers of MNPs, which may limit the direct comparability of the cells we describe to most MNP studies that define them first by their presence of surface H2-A.

In vitro experiments with bone-marrow-derived MNPs offer a useful alternative to *in vivo* experiments that may not be feasible, but given the importance of local tissue signals for MNPs and expected differences of *in vitro* skewed cells, results from *in vitro* assays are not expected to always reflect *in vivo* states. BMDCs from GM-CSF skewed bone marrow did not appear to acquire H2-A from MODEK cells *in vitro* (Figure 6B), yet *in vivo* DCs frequently acquired membrane from IECs (Figure 7A) and exhibited less surface H2-A in $IEC^{\Delta MHCII}$ mice (Figure 4D). This could be attributed to differences between BMDCs and primary siLP DCs, differences between immortalized MODEK cells and ileum IECs, or lack of other cell types present in the siLP. Future *in vitro* studies with enteroid-derived gut monolayers and more specific subsets of primary DCs will help dissect the role of MNP subsets in transferring IEC-derived proteins and their functional differences.

Author Manuscript Author Manuscript Author Manuscript Author Manuscript

The lack of IEC MHC class II resulted in increased colon pathology as assessed by histological scoring but not by colon length or weight loss in a DSS-induced model of colitis (Figures 3C-3F). Another group using this $IEC^{\Delta MHCII}$ mouse has now reported the opposite colon histology pattern in a DSS-recovery model but also did not see a weight change and found increased histological inflammation scores and decreased sIgA bacterial opsonization in a *C. rodentium* model of colitis (Jamwal et al., 2020). DSS colitis mainly effects the colon but highest MHC class II expression at steady state is in the ileum (Figures 1A and 1B). However, if MHC class II molecules are transferred to migratory MNPs that also interact with migratory T cells, colonic involvement is not unexpected, although the exact mechanism is unclear. Additionally, if H2-A transfer constrains the microbiota, which is intimately involved in colitis and varies between animal facilities, differences in colitis severity are also not unexpected. Future studies should use gnotobiotic mice with defined communities, assess colonic MHC class II levels during disease models, and further assess immune cell trafficking and immune repertoire development in these models. We provide correlative evidence that B cell repertoires are less selected without IEC MHC class II, yet determining the exact mechanistic point where IEC-transferred MHC class II impinges on BCR selection requires further investigation.

STAR★METHODS

RESOURCE AVAILABILITY

Lead contact—Further information and requests for resources, reagents and additional information should be directed to the lead contact, June L.

Round (june.round@path.utah.edu)

Materials availability—This study did not generate new unique reagents.

Data and code availability

- Raw and processed RNA-seq and single-cell RNA-seq (scRNaseq) have been deposited at GEO and are publicly available as of the date of publication. Raw and processed 16S rRNA gene sequencing data have been deposited at SRA and Zenodo, respectively, and are publicly available as of the date of publication. Accession numbers are listed in the key resources table. Microscopy data reported in this paper will be shared by the lead contact upon request.
- All original code has been deposited at Zenodo and is publicly available as of the date of the publication. DOIs are listed in the key resources table.
- Any additional information required to reanalyze the data reported in this paper is available from the lead contact upon request.

EXPERIMENTAL MODELS AND SUBJECT DETAILS

Mice—All mice described in these studies were on the C57BL/6J genetic background with the exception of the GF mice data shown in Figures 1D-1F which used Swiss Webster (SW) mice. Mice were housed in animal facility at the University of Utah and all experiments

Author Manuscript Author Manuscript Author Manuscript Author Manuscript

were in adherence to federal regulations as well as the guidelines for animal use set forth by the University of Utah Institutional Animal Care and Use Committee. Mice were age- and sex-matched for all experiments and mice from both sexes are reported in the data, but analysis of sex-specific differences was not performed. We used 8-16 week old mice for all experiments except for individually housed animals assessed from 4-7 weeks old in Figure 2E. Animals were genotyped prior to weaning at 3 weeks of age and separated by sex and genotype at weaning except where we have noted they were cohoused by genotypes. *H2-Ab1*$^{loxP/loxP}$ mice (Jackson Laboratories, stock # 013181) were crossed with *Villin*:Cre mice (Jackson Laborartories, stock # 004586) to obtain IEC$^{\Delta MHCII}$ mice. Due to known low-level testes expression of Cre recombinase in *Villin*:Cre mice, breeder pairs were always maintained as female *H2-Ab1*$^{loxP/loxP}$; *Villin*:Cre$^{Tg/-}$ (i.e., IEC$^{\Delta MHCII}$) with male *H2-Ab1*$^{loxP/loxP}$; *Villin*:Cre$^{-/-}$ (i.e., "WT") to prevent germline knockouts from occurring, and to allow comparison of WT and IEC$^{\Delta MHCII}$ among littermates. All mice were genotyped for the presence of the *Villin*:Cre construct, as well as the first *H2-Ab1* exon that is flanked by loxP sites in these mice to ensure germline deletions were not present. Additionally, IEC H2A phenotype was confirmed by flow cytometry of epithelial cells for all experiments. We improved on the supplier-provided genotyping protocol for *Villin*:Cre by using primers that spanned the *Villin* gene promoter and Cre junction. The *Villin*:Cre targeting forward primer (5′-ACCCCCATAGGAAGCCAGTT-3′) and reverse primer (5′-GTTTTTACTGC CAGACCGCG-3′) were used in conjunction with internal positive control primers (Jackson lab primers oIMR7338/oIMR7339; 5′-CTAGGCCACAGAATTGAAAGATCT-3′ / 5′-GTAGGTGGAAATTCTAGCATCATCC-3′) to yield an approximately 450 base-pair fragment for *Villin*:Cre-positive mice with a 324 base-pair fragment for the internal positive control. The amplification program was as follows: 95°C for 2 minutes, 35 cycles of 95°C for 20 s, 62°C for 15 s, 72°C for 20 s, and a final 2 minute extension at 72°C. To obtain the T cell-deficient mice with IEC-conditional *H2-Ab1* knockout (TCRβ−/−; IEC$^{\Delta MHCII\ or\ wT}$), we crossed the IEC$^{\Delta MHCII}$ to *Tcrb*$^{-/-}$ knockout mice (Jackson Laboratories, 002118) and interbred to obtain homozygous *Tcrb*$^{-/-}$ knockouts and homozygous *H2-Ab1* floxed mice, then maintained them with breeder pairings as described for IEC$^{\Delta MHCII}$ animals with respect to the *Villin*:Cre. The *Tcrb* knockout was genotyped with the standard PCR genotyping protocol provided by Jackson Laboratories. *H2-Ab1*$^{-/-}$ total body knockout mice on the C57BL/6 background were purchased from Taconic (Taconic, cat # ABBN12). mT/mG mice were obtained from Jackson Laboratories (stock # 007676) and crossed to the same *Villin*:Cre mice used in all other experiments. 10-12 week old NSG-Ab DR4 mice carrying the human HLA-DR4 transgene were purchased from Jackson Laboratories (stock # 017637) and used immediately as bone marrow donors. OT-II transgenic mice (stock # 004194) and CD45.1 mice (stock # 002014) were purchase from Jackson Laboratories and crossed to create OT-II;CD45.1 donor-mice which were confirmed by genotyping according to Jackson lab's protocol for the OT-II transgenes and blood phenotyping with anti-CD45.1 and anti-CD45.2 antibodies (Tonbo Biosciences, clone A20 and clone 104).

Cell lines and primary cell cultures—MODEK cells previously described were maintained, and associated with MNPs, in DMEM media with L-glutamine, 4.5g/L glucose and sodium pyruvate supplemented with 10% v/v FBS, 1X penicillin-streptomycin and 1X non-essential amino acids at 37°C (Vidal et al., 1993). Primary sorted, or bone-marrow

Author Manuscript Author Manuscript Author Manuscript Author Manuscript

derived, MNP cells obtained from female *H2-Ab1*$^{-/-}$ mice were added to stimulated MODEK cells (directly on MODEK cells or in lower well without MODEK cells for transwell assays) and further incubated under MHCII-stimulating conditions (with fresh media) for 24 hours before staining and assaying by flow-cytometry. Bone marrow-derived cells from female *H2-Ab1*$^{-/-}$ mice were skewed by adding GM-CSF for BMDCs or M-CSF for BMMs at a concentration of 20 ng/ml after 3 days in culture and then maintained under skewing conditions for 4 more days before being split and used in MODEK associations 2 days later. Additional details of the plating density and growth conditions during association with MNPs is found in the methods details section under *in vitro* cell associations.

METHOD DETAILS

Tissue dissection and cell isolation—Lamina propria cells, epithelial cells and lymphoid tissue cells were isolated as we have previously described, with minor modifications intended to increase viable epithelial cell recovery and avoid potential differential representation of cells due to the use of Percoll gradients that have now been shown to be unnecessary (Kubinak et al., 2015a; Goodyear et al., 2014). Briefly, after euthanization with CO_2 and cervical dislocation, mLNs, whole small intestines and/or colons were first dissected. We defined the most distal 10 cm of small intestines as ileum and this was cut away from the rest of the small intestine after removing Peyer's patches along the entire length of the SI. Visible mesentery was carefully removed from the intestines which were then cut open longitudinally and gently scraped with the back of forceps to remove loosely adherent mucus and intestinal contents. These opened intestines were first rinsed for 10 minutes at 4°C with shaking in 10 mL of 1X HBSS (without Ca^{2+} and Mg^{2+}) containing 1.5 mM DTT and 10 mM HEPES. After rinse, tissue was removed and cut into small pieces then placed in dissociation solution (HBSS without Ca^{2+}/Mg^{2+} containing 1.5 mM DTT, 10 mM HEPES and 30 mM EDTA), and shaken for 25 minutes at 37°C. Dissociated IECs were collected after incubation by first giving 10 horizontal shakes of the tissues and vortexing for 10 s, then passing the tissue over a 100 μM cell-strainer. The flow-through containing IECs was then passed over a 40 μM cell strainer, rinsed with 10 mL of 1X sterile PBS and the flow-through containing IECs collected. This flow-through was spun down for 5 minutes at 400 x g and rinsed 1X with column buffer then resuspended in column buffer (HBSS without Ca^{2+}/Mg^{2+} containing 2 mM EDTA, 0.5% FBS, 10 mM HEPES) and cells counted. The tissue collected on the first 100 μM cell-strainer contained lamina propria and this was processed in parallel by first incubating tissue for 25 (SI) or 45 (colon) minutes at 37°C in 15 mL of LP digestion solution (HBSS plus Mg^{2+}/Ca^{2+} and 2.5% v/v FBS with 50 U/ml Dispase II, 0.5 mg/ml DNase I and 0.5 mg/ml Collagenase D). After incubation, the tissue was vortexed and passed over a 40 μM cell strainer then rinsed with 10 mL 1X PBS to collect liberated LP cells in the flow-through. The flow-through was then spun down for 10 minutes at 500 x g, supernatant poured off and cells gently resuspended in 10 mL column buffer and moved to new tubes. The cells were then spun down as before and rinsed again with 10 mL column buffer and then finally resuspended in 0.5 mL column buffer before counting and staining. Notably, as opposed to our previously described method, no Percoll gradient was used. mLN and Peyer's patches were placed in 40 μM cell strainers in complete RPMI following dissection. Subsequently, the tissues were broken up on the cell-strainers with plungers from sterile 1 mL syringes and cells that passed

Author Manuscript Author Manuscript Author Manuscript Author Manuscript

through the strainers were collected, spun down for 5 minute at 367 x g, resuspended in complete RPMI and counted before staining.

DSS treatment and pathology scoring—Acutes DSS-induced colitis was induced by providing 3% (w/v) DSS (MP Biomedicals) in drinking water for 6 days. Fresh DSS solution was provided twice during the 6 day administration. Animal weights were obtained before DSS treatment and mice were monitored for weight change daily throughout the experiments. For histology, entire colons were dissected from below the cecum to rectum, lumenal contents flushed out and the tissue fixed in formalin before being embedded, sectioned and H&E stained by the University of Utah Research Histology core. Slides were scored for crypt loss and inflammation as we have previously detailed and the aggregate pathology score was reported (Kubinak et al., 2015a).

Bone marrow and T cell transfer experiments—For MHC-mismatched adoptive transfer experiments, 5 female NSG-Ab DR4 donor mice were euthanized and bone marrow was harvested from the hind limb bones by centrifugation (30 s at 10,000 x g) after removing muscle and connective tissue as previously described (Amend et al., 2016). Bone marrow cells were resuspended in sterile HBSS (without Ca^{2+} / Mg^{2+}) at a density of $1.9x10^7$ cells per ml and 200 μL ($3.8x10^6$ cells) was tail-vein injected into host mice (*TCRb−/−;* $IEC^{\Delta MHCII \text{ or } WT}$) immediately following their second dose of radiation. Host mice were irradiated twice with 450 rads separated by 4 hours. For adoptive transfer of OT-II T cells, donor CD4+ T cells were isolated from spleens of OT-II mice with a MACS CD4+ T cell isolation kit and $4.2x10^6$ cells resuspended in 50 μL HBSS (without Ca^{2+} / Mg^{2+}) was retro-orbitally injected into WT and $IEC^{\Delta MHCII}$ host-mice following a single dose of irradiation with 400 rads. OVA (Ovalbumin) was then provided in drinking water at a concentration of 1 mg/ml and changed every 2-3 days for 3 weeks after transfer.

Fecal immunoglobulin assays—Fecal IgA and IgG were quantified using ELISA kits (ThermoFisher Scientific) from fecal supernatants prepared as previously described (Kubinak et al., 2015a). Bacteria bound by immunoglobulins were analyzed by flow cytometry of washed fecal pellets stained with SYBR green I and rat anti-mouse IgA (eBioscience clone mA-6E1, PE), anti-mouse IgG1 (Santa Cruz, CruzFluor 555) or anti-mouse IgG3 (Santa Cruz, CruzFlour 555) as previously described (Kubinak et al., 2015a).

Flow cytometry and antibody panels—All end-point flow cytometry analyses were performed on a BD LSR Fortessa instrument and all cell sorting was performed on a BD FACSAria instrument with a 100 μm nozzle. Positive cell populations were identified with the use of FMO (fluorescence minus one) or appropriate isotype controls and viable cells were identified with the use of Ghost Dye Violet 510 or Red 780 (Tonbo Biosciences). FCS files were analyzed with FlowJo (v10) software to identify populations and create count matrices. The I-A/I-E antibody (clone M5/114.15.2) was used for detecting H2-A (MHCII) on all experiments except when distinguishing different haplotypes. To detect MODEK cell-derived H2-A we used the $H2^k$ haplotype-reactive antibody $I\text{-}A^k$ (BioLegend, clone 10-3.6). To distinguish mouse and human MHCII in bone marrow transfer studies we used a mouse $H2^b$ haplotype-specific antibody (Biolegend, clone AF6-120.1) and a human

Author Manuscript Author Manuscript Author Manuscript Author Manuscript

HLA-DR specific antibody (Tonbo, clone L243). All antibodies were used at 1:250 (v:v) dilution in column buffer for cell stains unless otherwise noted. For cell antibody staining, cells were plated at $0.25x10^6$-$2x10^6$ cells per well of a 96 well plate, live/dead stained (if included) with 100 μL Ghost Dyes diluted 1:1000 (v:v) in PBS at room temperature for 20 minutes then rinsed once in column buffer. Fc receptors were blocked by adding 100 μL Fc Shield (diluted 1:250 (v:v) in column buffer; Tonbo Biosciences) and incubating for 20 minutes at 4°C. Antibody stains in 100 μL were added directly and cells incubated for another 20 minutes at 4°C, then rinsed twice in column buffer before fixing or running on flow cytometer. Antibody panels used for assays include: H2-Aon IECs (Figures 1 and 2A)(Ghost Violet 510, EpCAM APC, I-A/I-E PE (H2-A), CD45 PECy7), Tregs (Figures 3A, 3B, and 3G)(CD3 violet-Fluor450 or CD3e Pacific Blue, CD4 FITC, Foxp3 APC, Helios PerCP-Cy5.5, RORγt eFluor610), MNPs (Figures 4C-4F)(Dump PerCP-Cy5.5[CD3, CD19, NK1.1, Ly-6G], CD45 violetFluor450, CD11b PE-Cy7, CD11c SuperBright600, CX3CR1 PE/Dazzle594, Ly-6C AlexaFluor488, I-A/I-E APC, CD64 BV711, CD103 PE), Primary *H2-Ab1*$^{-/-}$ MNPs after MODEK cells association (Figure 6C)(I-A^k PE, CD45 violetFluor450, Ly-6C AlexaFluor488, CD64 BV711, CX3CR1 BV510, CD103 APC-Cy7), *H2-Ab1*$^{-/-}$ BMM/BMDCs after MODEK cells association (Figure 6B)(I-A^k PE, CD45 violetFluor450, CD11c FITC, CX3CR1 BV510), OT-II associated with OVA-pulsed MNPs (Figure 6D)(CD45.1 PE, CD3 violetFluor450, Foxp3 APC, CFSE), mTmG mice assayed with Fortessa (Figure 7A)(Dump PerCP-Cy5.5[CD3, CD19, NK1.1, Ly6G], CD45 violetFluor450, CD11b PE-Cy7, CD11c SuperBright600, I-A/I-E APC, CD64 BV711, CD103 APC-Cy7), mTmG mice assayed with ImageStream (Figure 7B)(Ghost Violet 510, Dump APC-Cy7 [CD3e, IgM], CD45 violetFluor450, I/A-IE APC, GFP, tdTomato), MHCII chimeras (Figures 7C and 7D)(Dump PerCP-Cy5.5[CD3, CD19, NK1.1, Ly-6G], CD45 violetFluor450, CD11b PE-Cy7, CD11c SuperBright600, CX3CR1 PE/Dazzle594, CD64 BV711, Ly-6C AlexaFluor488, I-Ab APC, HLA-DR PE), Tfh and Tfr (CD3 PerCP-Cy5.5, CD4 violetFluor450, Foxp3 APC, CXCR5 PE, PD-1 PE-Cy7), OT-II Tfh and Tfr (CD4violetFluor450, CD45.1 FITC, PD-1 PE-Cy7, CXCR5 PE, Foxp3 APC, Helios PerCP-Cy5.5), germinal center B cells (IgD AlexaFluor647, GL-7 FITC, B220 PerCP-Cy5.5, FAS PE-Cy7).

FITC-dextran permeability assays—Assessment of intestinal barrier using FITC-dextran (3,000-5000 MW) was performed similarly to previously described, except mice were fasted overnight (with water provided) instead of only 4 hours before FITC-dextran gavage (Chiaro et al., 2017). 6 μL of FITC-dextran (100 mg/ml in PBS) per gram of body weight was gavaged the morning after fast and followed by 4 more hours of fasting before sacrifice and blood collection. PBS only gavages were given to 2-3 mice as controls to normalize to background signal. Blood was taken by cardiac puncture, allowed to sit 30 minutes at room temperature and then centrifuged at 1500 x g for 10 minutes and the serum supernatant was removed to a new tube. Serum was diluted 1:2 and 1:10 (v/v) with PBS (to ensure a reading within the dynamic range of the plate reader) and 100 μL was assayed in black flat-bottom 96 well plates on a microplate reader with 488 nm excitation and 519 nm emission (Biotek Synergy H1). Average values from duplicates of ten 2-fold dilutions of FITC-dextran diluted in PBS (1 mg/ml starting concentration) were used as standards to

Author Manuscript Author Manuscript Author Manuscript Author Manuscript

generate a standard curve and extrapolate values of FITC-dextran in the serum, and values were expressed as fold-change over serum from PBS-only gavaged mice.

Immunofluorescent histochemistry—10 cm of the distal small intestine was dissected and lumenal contents gently pushed out with the back of forceps before fixing the tissue in 5 mL of 10% buffered formalin solution for 4 hours at room temperature with rocking. Tissue was then rinsed 3 times for 5 minutes each in PBS at room temperature and then placed in 30% (w/v) sucrose overnight at 4 C with rocking. Samples were then embedded and cryosectioned in 9 μm thick sections by the University of Utah Research Histology core. Frozen sections were stored at −70 C until staining. An antigen retrieval step was performed to begin staining of sections for H2-A / MHCII. First, sections were warmed to room temperature, rinsed once in PBS for 10 minutes then transferred to prewarmed (95 C) containers with 10mM citric acid (pH 6.0) and incubated at 95 C for 20 minutes. Containers with slides were then cooled to room temperature and rinsed twice for 5 minutes each in PBS. Sections were blocked for 1 hour at room temperature using a blocking solution of 3% (v/v) goat serum, 5% (w/v) BSA, 0.01% Na-Azide (w/v) and 0.1% (v/v) Triton X-100 made in PBS (without Ca^{2+} and Mg^{2+}). Primary labeled anti-mouse I-A/I-E (H2-A) AlexaFluor 647 was then added (diluted 1:250 in blocking solution) and slides incubated overnight at 4 C. Slides were then rinsed 5 times for 5 minutes each at room temperature with PBS. Counterstains with either DAPI alone or DAPI and Phalloidin-conjugated with fluorescent dye 555-I (Abnova) were added to slides and incubated for 10 minutes at room temperature followed by 2 more rinses in PBS before mounting with Vectashield hard set mounting reagent.

Imaging flow cytometry—Tissue samples from mT/mG and Villin:Cre; mT/mG mice were prepared as described for standard flow cytometry. Half of each sample was analyzed with an overlapping, but more extensive, antibody panel on a BD LSR Fortessa (Figures 7A and 7B) and the other half analyzed with the Amnis ImageStream Mk II platform (405, 488, 561,642 and 785 nm excitation lasers; 60X magnification) and ISX software (version 201.1.9.725) using the highest bin mode resolution. Data was then processed with IDEAS software (version 6.3). Cells were first gated based on their brightfield gradient RMS as a measure of focus, followed by their area and aspect ratio to exclude debris and aggregates. CD45+ MHCII+ cells were interrogated for tdTomato surface staining and GFP+ puncta. Fluorescent channel brightness was normalized to the brightest cell per fluorochrome within the CD45+ MHCII+ population.

Single cell RNaseq—Cells from PP and siLP of 4 female WT and 4 female $IEC^{\Delta MHCII}$ were collected as described in tissue dissection and cell isolation section, except DNase was not included in the siLP digestion and the digestion time was increased to 45 minutes. After tissue digestion (for siLP) the cells were washed one more time with column buffer and the isolated cells (from both siLP and PP) were enriched for $CD45^+$ cells using MACS columns with $CD45^+$ microbeads. The collected $CD45^+$ cells from each animal were counted and evenly mixed to provide a single sample of each genotype from each tissue. The University of Utah High-throughput Genomics core then prepared 5′ gene expression and

Author Manuscript Author Manuscript Author Manuscript Author Manuscript

VDJ profiling libraries (from the same cells) with the 10X genomics platform, and libraries were run on an Illumina NovaSeq instrument.

Bulk RNaseq—For RNaseq of sorted epithelial cells, the dissociation fraction of ileal lamina propria preps was used to sort Live, $CD45^{-}$, $EpCAM^{+}$ cells from WT and $IEC^{\Delta MHCII}$ mice. After dissociation described in the tissue dissection section, cells were spun down at 367 x g, rinsed once with 5 mL of HBSS, counted and resuspended at a concentration of 1×10^6 cells per 100 μL Ghost Dye Red 780 (Tonbo Biosciences) diluted to 1 μL per ml in HBSS and incubated for 10 minutes in the dark at 4°C. Following incubation, 100 μL of labeled antibodies diluted 1:500 in column buffer (EpCAM eFluor450, CD45 PE) were added and cells were incubated for an additional 20 minutes in the dark at 4°C. Cells were then washed twice in column buffer and resuspended in complete RPMI and kept on ice until sorting. 400,000 epithelial cells from each animal were sorted into tubes with complete RPMI using a BD FACS Aria at the University of Utah Flow Cytometry core. Sorted cells were then spun down at 367 × g for 5 minutes and resuspended in 600 μL TRIzol. RNA was extracted with Direct-zol RNA Microprep kits (Zymo Research, cat # R2062) as per manufacturer's instructions and eluted with 16.5 μL elution buffer. RNA was quantified with the nanodrop and ranged from 32 - 132 ng/μl. For RNaseq of ileal tissue during DSS colitis, the most distal 2 cm of ileum (without Peyer's Patches) was dissected, cut open longitudinally and gently scraped with forceps to remove any lumenal contents, then placed in TRIzol and stored at −80°C until RNA extraction with Direct-zol RNA microprep kits after bead-beating with 2.8 mm ceramic beads for 2 minutes with a Mini-Bead-Beater 16 (BioSpec Products). For the sorted lECs RNA-seq, sequencing libraries were prepared from RNA by the University of Utah High-throughput genomics core using the Illumina TruSeq Stranded RNA kit with Ribo-Zero Gold. For RNA-seq of DSS-treated ileal tissue, libraries were prepared with NEBNext Ultra II Directional RNA Library Prep kit for Illumina. For each project, individual samples were multiplexed and sequenced on a single lane of an Illumina HiSeq 2500 instrument with 50 cycle single-end reads. All raw sequences have been deposited in the NCBI SRA under BioProject accession PRJNA758100 and GEO with accession listed in the Key Resources Table.

16S sequencing—Fecal pellets or ileal contents were collected individual mice and immediately frozen at −70°C in 2mL screw cap tubes containing 250 mg of 0.15 mm garnet beads (MoBio, cat# 13122-500). DNA was extracted using the Power Fecal DNA Isolation Kit (MoBio or QIAGEN), per kit instructions and included 2 cycles of 1 minute of bead beating at 4°C on a Mini-Bead-Beater 16 (BioSpec Products). 16S rRNA gene amplification of the V3 and V4 regions with the addition of dual indices described by Kozich, cleaning and multiplexing was done as we have previously described (Kubinaket al., 2015a; Kozich et al., 2013). This method used a single PCR (performed in triplicate for each sample) with primers that contained (described 3′ to 5′) the V3/4 region 16S rRNA gene targeting sequence, then a 2-nucelotide pad followed by the Illumina adaptor sequences and an 8-nucleotide index sequence. The V3/4 16S rRNA gene targeting sequences were those described by Kubinak for all experiments except for the ileal sequencing described in Figures 2F-2H, for which we used the V3/4 16S-targeting sequences described by Takahashi (Takahashi et al., 2014; Kubinak et al., 2015a). The full oligonucleotide sequences are

Author Manuscript Author Manuscript Author Manuscript Author Manuscript

reported in the Key Resources table with indices denoted by Xs. Individual sequencing libraries were multiplexed across 4 different runs and sequenced on an Illumina MiSeq instrument in paired-end 300 cycle mode.

qPCR—Ileal tissue (2 cm most distal) was dissected and stored in TRIzol in 2 mL screw-cap tubes prior to RNA isolation. Ceramic beads (2.8 mm, Omni International) were added to tubes and then the tissue was bead-beaten for 2 minutes with a Mini-Bead-Beater 16 (BioSpec Products). Total RNA was then isolated using Direct-zol RNA purification kits and cDNA was synthesized with qScript cDNASuperMix (QuantaBio). qPCR reactions were performed on a Roche LightCycler480 using LightCycler480 SYBR Green I master mix (Roche). All assays were normalized to expression level of Rpl32. The primer sequences used were: Rpl32_F(5′-AAGCGAAACTGGCGGAAAC-3′), Rpl32_R(5′-TAACCGATGTTGGGCATCAG-3′), Tjp1_F(5′-GCCGCTAAGAGCACAGCAA-3′), Tjp1_R(5′-TCCCCACTCTGAAAATGAGGA-3′), Tjp2_F(5′-ATGGGAGCAGTACACCGTGA-3’), Tjp2_R(5′-TGACCACCCTGTCATTTTCTTG-3′), Tjp3_F(5′-CTGTGGAGAACGTCACATCTG –3′), Tjp3_R(5′-TTGGCTGTTTTGGTGCAGGT –3′), Cldn7_F(5′-GGCCTGATAGCGAGCACTG –3′), Cldn7_R(5′-GTGACGCACTCCATCCAGA –3′), Cldn2_F(5′-CAACTGGTGGGCTACATCCTA-3′), Cldn2_R(5′-CCCTTGGAAAAGCCAACCG-3′). Primers were synthesized by the University of Utah DNA synthesis core.

***In vitro* cell associations—**For MNP-associations with MODEK cells, 48 hours before association the MODEK cells were resuspended, counted and then seeded at an initial density of 50,000 cell per ml into standard 24-well plate wells with 500 μL of cell suspension, or into transwell inserts with 90 μL cell-suspension (and 600 μL media only in the lower well), to maintain the same surface-area cellular density in both conditions. This seeding density was found to be optimal such that MODEK cells were not already confluent when the MNPs were added. To stimulate MHCII expression in MODEK cells, recombinant mouse IFNg was added at a final concentration of 100 ng/ml along with Pam3CSK4 at a concentration of 1 μg/ml at initial seeding, which we found to be an even more potent stimulator of MHCII on MODEK cells than IFNγ alone (data not shown). Primary sorted, or bone-marrow derived, cells obtained from female *H2-Ab1*$^{-/-}$ mice were added to stimulated MODEK cells (directly on MODEK cells or in lower well without MODEK cells for transwell assays) and further incubated under MHCII-stimulating conditions (with fresh media) for 24 hours before staining and assaying by flow-cytometry. Primary isolated, sorted cells pooled from 7 female 9-weekold *H2-Ab1*$^{-/-}$ mice were added at a density of 3,000 - 5,000 cells per well, while BMDCs/BMMs were added at a density of 20,000 cells per well. To collect cells for staining, the cells were scraped from wells and pipetted up and down with a wide-bore 1 mL pipette tip to avoid enzymatic degradation of surface proteins. Bone marrow-derived cells from *H2-Ab1*$^{-/-}$ mice were skewed by adding GM-CSF for BMDCs or M-CSF at a concentration of 20 ng/ml after 3 days in culture and then maintained under skewing conditions for 4 more days before being split and used in MODEK associations 2 days later.

Author Manuscript Author Manuscript Author Manuscript Author Manuscript

For association of OT-II T cells and MNPs, spleens from OT-II mice were first collected and CD4+ cells isolated with a MACS column and CD4+ T cell isolation kit. OT-II cells were then labeled with CFSE in DPBS + 0.05% (w/v) BSA for 10 minutes in a 37°C incubator, rinsed twice with complete RPMI culture media, then resuspended and plated in 96-well v-bottom plates at a density of 60,000 cells per well along with 6,000 OVA-pulsed MNPs. Primary isolated and sorted MNP cells were pulsed with OVA(329-337) peptide prior to association with OT-II cells by incubating them with 10 μM peptide for 45 minutes in a 37°C tissue incubator. Then, the OVA-pulsed cells were rinsed twice with complete RPMI and mixed with the CFSE-labeled OT-II cells in a separate plate and incubated together for 72 hours before assay.

Bone marrow and T cell transfer experiments—For MHC-mismatched adoptive transfer experiments, 5 female NSG-Ab DR4 donor mice were euthanized and bone marrow was harvested from the hind limb bones by centrifugation (30 s at 10,000 x g) after removing muscle and connective tissue as previously described (Amend et al., 2016). Bone marrow cells were resuspended in sterile HBSS (without Ca^{2+} / Mg^{2+}) at a density of $1.9x10^7$ cells per ml and 200 μL ($3.8x10^6$ cells) was tail-vein injected into host mice (*TCRb*−/−; $IEC^{\Delta MHCI1 \text{ or } WT}$) immediately following their second dose of radiation. Host mice were irradiated twice with 450 rads separated by 4 hours prior to injection. For adoptive transfer of OT-II T cells, donor CD4+ T cells were isolated from spleens of OT-II mice with a MACS CD4+ T cell isolation kit and $4.2x10^6$ cells were resuspended in 50 μL HBSS (without Ca^{2+}/ Mg^{2+}) then retro-orbitally injected into WT and $IEC^{\Delta MHCII}$ host-mice following a single dose of irradiation with 400 rads. OVA (Ovalbumin) was then provided in drinking water at a concentration of 1 mg/ml and changed every 2-3 days for 3 weeks after transfer.

QUANTIFICATION AND STATISTICAL ANALYSIS

Bioinformatics processing of sequence data—16S rRNA gene raw reads were processed and analyzed within the QIIME2 framework (2019.4) (Bolyen et al., 2019). Demultiplexed and quality-filtered sequences were first trimmed of primer and linker sequences with the Cutadapt plugin, then joined with vsearch, trimmed to 392 nucleotides and denoised with Deblur (Martin, 2011; Rognes et al., 2016; Amir et al., 2017). Chimeras were filtered with uchime-denovo method in the vsearch plugin and taxonomies assigned with the classify-sklearn method in the feature-classifier plugin, against the Greengenes reference set (13_8) trimmed to the amplified region and trained with the fit-classifier-naive-bayes method (Pedregosaet al., 2011; Bokulich et al., 2018). Diversity metrics, distances and statistical significance of beta diversity groupings by permanova were calculated within QIIME2 (Anderson, 2001). All code used for processing of 16S data, as well as the processed ASV tables, taxonomies and phylogenies are available at Zenodo with the DOI shown in the Key Resources table.

For bulk RNA-seq from ileal tissue treated with DSS, raw reads were aligned to the mouse assembly GRCm38.89 (mm10) using TopHat2 and per gene aligned read counts for each sample were collated and filtered of genes with less than 2 reads aligning using the R package GenomicAlignments (Lawrence et al., 2013; Kim et al., 2013). For bulk RNA-seq

Author Manuscript Author Manuscript Author Manuscript Author Manuscript

of sorted lECs, raw reads were aligned to the mm10 transcriptome using Novoalign and counts were generated using USeq's DefinedRegionDifferentialSeq application. For both bulk RNA-seq projects, the resultant count matrices were uploaded and analyzed with the BioJupies framework for differential expression testing and term enrichment tests (Torre et al., 2018). Volcano plots were made in R from the differential expression table values generated by BioJupies which utilized Limma for differential expression analysis (Ritchie et al., 2015).

scRNaseq Illumina reads were initially processed using the 10X Genomics Cell Ranger pipeline against the mouse GRCm38 reference assembly, then further analyzed with the Seurat package in R (Butler et al., 2018). We initially filtered out cells that had less than 200 genes detected and genes that were found in less than 5 cells, then filtered cells with higher than 8% mitochondrial reads to exclude low-quality dying cells. We then regressed out the effect of UMI (unique molecular identifier) and mitochondrial gene representation prior to further analysis. Differential expression signatures for cell clusters after combining samples were uploaded to the CIPR tool and used against the mouse ImmGen reference set to annotate cell types of each cluster (Ekiz et al., 2020). Some cell types, particularly in the siLP, had an ambiguous identity score and were manually annotated based on a combination of CIPR identification and direct examination of differentially expressed genes. Cell Ranger vdj was used to process VDJ sequences and the resulting clonotypes count tables were imported in to R. The vegan package in R was used to rarefy without replacement to an even number of observations and to calculate Shannon diversity (Oksanen et al., 2019). The Change-O package within the Immcantation framework was used to import 10X genomics data and assess mutation rates after collapsing cells into clonotypes for each of the detected antibody isotypes (Gupta et al., 2015).

STATISTICAL ANALYSIS

Statistical analyses was performed using GraphPad Prism for all flow cytometry data, ELISA data and qPCR. RNAseq statistics were calculated within BioJupies. 16S sequencing statistics were calculated with QIIME2 plugins (permanova and ANCOM) or within R (anosim using the vegan package) (Mandal et al., 2015; Oksanen et al., 2019). Error bars indicate standard deviation in all graphs and mean or median as noted in figure legends. Error bars in SuperPlots of replicate data indicate SD of replicates (Lord et al., 2020). MFI for flow cytometry data is the median fluorescent intensity. For all figures significance was defined and denoted as * $p < 0.05$; ** $p < 0.01$; *** $p < 0.001$; **** $p < 0.0001$. Number of animals used or replicates (n), as well as the corresponding statistical tests used, are denoted in the methods or figure legends.

Supplementary Material

Refer to Web version on PubMed Central for supplementary material.

ACKNOWLEDGMENTS

This work was supported by an NSF CAREER award (IOS-01253278), a Pack-ard Fellowship in Science and Engineering, and the Crohn's and Colitis Foun-dation Senior Research Awards to J.L.R., aswell as NIH grant R01-AI123106– 01 to R.M.O. J.L.K. was supported by K22AI123481, R21AI142409, and R0AI155887.

Author Manuscript Author Manuscript Author Manuscript Author Manuscript

K.M.B. was supported by NIH T32 AI138945–1. This work was supported by the University of Utah Flow Cytometry Facility in addition to the National Cancer Institute through Award 5P30CA042014–24 and NIH Award Number 1S10RR026802–01. The Center for High Performance Computing at the University of Utah is gratefully acknowledged.

REFERENCES

Amend SR, Valkenburg KC, and Pienta KJ (2016). Murine hind limb long bone dissection and bone marrow isolation. J. Vis. Exp 10, 53936.

Amir A, McDonald D, Navas-Molina JA, Kopylova E, Morton JT, Zech Xu Z, Kightley EP, Thompson LR, Hyde ER, Gonzalez A, and Knight R (2017). Deblur Rapidly Resolves Single-Nucleotide Community Sequence Patterns. mSystems 2, e00191–e16. [PubMed: 28289731]

Anderson MJ (2001). A new method for non-parametric multivariate analysis of variance. Austral Ecol. Published online June 28, 2008. 10.1111/j.1442-9993.2001.01070.pp.x.

Atarashi K, Tanoue T, Oshima K, Suda W, Nagano Y, Nishikawa H, Fukuda S, Saito T, Narushima S, Hase K, et al. (2013). Treg induction by a rationally selected mixture of Clostridia strains from the human microbiota. Nature 500, 232–236. [PubMed: 23842501]

Bain CC, and Schridde A (2018). Origin, differentiation, and function of intestinal macrophages. Front. Immunol 9, 2733. [PubMed: 30538701]

Bär F, Sina C, Hundorfean G, Pagel R, Lehnert H, Fellermann K, and Büning J (2013). Inflammatory bowel diseases influence major histocompatibility complex class I (MHC I) and II compartments in intestinal epithelial cells. Clin. Exp. Immunol 172, 280–289. [PubMed: 23574324]

Biton M, Haber AL, Rogel N, Burgin G, Beyaz S, Schnell A, Ashenberg O, Su CW, Smillie C, Shekhar K, et al. (2018). T Helper Cell Cytokines Modulate Intestinal Stem Cell Renewal and Differentiation. Cell 175, 1307–1320. [PubMed: 30392957]

Bland PW, and Warren LG (1986). Antigen presentation by epithelial cells of the rat small intestine. II. Selective induction of suppressor T cells. Immunology 58, 9–14. [PubMed: 2423441]

Boehm F, Martin M, Kesselring R, Schiechl G, Geissler EK, Schlitt HJ, and Fichtner-Feigl S (2012). Deletion of Foxp3^{+} regulatory T cells in genetically targeted mice supports development of intestinal inflammation. BMC Gastroenterol. 12, 97. [PubMed: 22849659]

Bokulich NA, Kaehler BD, Rideout JR, Dillon M, Bolyen E, Knight R, Huttley GA, and Gregory Caporaso J (2018). Optimizing taxonomic classification of marker-gene amplicon sequences with QIIME 2's q2-feature-classifier plugin. Microbiome 6, 90. [PubMed: 29773078]

Bolnick DI, Snowberg LK, Caporaso JG, Lauber C, Knight R, and Stutz WE (2014). Major Histocompatibility Complex class IIb polymorphism influences gut microbiota composition and diversity. Mol. Ecol 23, 4831–4845. [PubMed: 24975397]

Bolyen E, Rideout JR, Dillon MR, Bokulich NA, Abnet CC, Al-Ghalith GA, Alexander H, Alm EJ, Arumugam M, Asnicar F, et al. (2019). Reproducible, interactive, scalable and extensible microbiome data science using QIIME 2. Nat. Biotechnol 37, 852–857. [PubMed: 31341288]

Britton GJ, Contijoch EJ, Mogno I, Vennaro OH, Llewellyn SR, Ng R, Li Z, Mortha A, Merad M, Das A, et al. (2019). Microbiotas from Humans with Inflammatory Bowel Disease Alter the Balance of Gut Th17 and RORγt^{+} Regulatory T Cells and Exacerbate Colitis in Mice. Immunity 50, 212–224. [PubMed: 30650377]

Büning J, Hundorfean G, Schmitz M, Zimmer K-P, Strobel S, Gebert A, and Ludwig D (2006). Antigen targeting to MHC class II-enriched late endosomes in colonic epithelial cells: trafficking of luminal antigens studied in vivo in Crohn's colitis patients. FASEB J. 20, 359–361. [PubMed: 16373401]

Büning J, von Smolinski D, Tafazzoli K, Zimmer K-P, Strobel S, Apostolaki M, Kollias G, Heath JK, Ludwig D, and Gebert A (2008). Multivesicular bodies in intestinal epithelial cells: responsible for MHC class II-restricted antigen processing and origin of exosomes. Immunology 125, 510–521. [PubMed: 18710406]

Butler A, Hoffman P, Smibert P, Papalexi E, and Satija R (2018). Integrating single-cell transcriptomic data across different conditions, technologies, and species. Nat. Biotechnol 36, 411–420. [PubMed: 29608179]

Author Manuscript Author Manuscript Author Manuscript Author Manuscript

Cerovic V, Houston SA, Scott CL, Aumeunier A, Yrlid U, Mowat AM, and Milling SWF (2013). Intestinal CD103(−) dendritic cells migrate in lymph and prime effector T cells. Mucosal Immunol. 6, 104–113. [PubMed: 22718260]

Chiaro TR, Soto R, Zac Stephens W, Kubinak JL, Petersen C, Gogokhia L, Bell R, Delgado JC, Cox J, Voth W, et al. (2017). A member of the gut mycobiota modulates host purine metabolism exacerbating colitis in mice. Sci. Transl. Med 9, eaaf9044. [PubMed: 28275154]

Chiba M, Iizuka M, and Masamune O (1988). Ubiquitous expression of HLA-DR antigens on human small intestinal epithelium. Gastroenterol. Jpn 23, 109–116. [PubMed: 3290039]

Cho K-J, Walseng E, Ishido S, and Roche PA (2015). Ubiquitination by March-I prevents MHC class II recycling and promotes MHC class II turnover in antigen-presenting cells. Proc. Natl. Acad. Sci. USA 112, 10449–10454. [PubMed: 26240324]

Cong Y, Feng T, Fujihashi K, Schoeb TR, and Elson CO (2009).A dominant, coordinated T regulatory cell-IgA response to the intestinal microbiota. Proc. Natl. Acad. Sci. USA 106, 19256–19261. [PubMed: 19889972]

Covassin L, Laning J, Abdi R, Langevin DL, Phillips NE, Shultz LD, and Brehm MA (2011). Human peripheral blood CD4 T cell-engrafted non-obese diabetic-scid IL2rγ(null) H2-Ab1 (tm1Gru) Tg (human leucocyte antigen D-related 4) mice: a mouse model of human allogeneic graft-versus-host disease. Clin. Exp. Immunol 166, 269–280. [PubMed: 21985373]

Cummings RJ, Barbet G, Bongers G, Hartmann BM, Gettler K, Muniz L, Furtado GC, Cho J, Lira SA, and Blander JM (2016). Different tissue phagocytes sample apoptotic cells to direct distinct homeostasis programs. Nature 539, 565–569. [PubMed: 27828940]

Cunningham AC, Zhang JG, Moy JV, Ali S, and Kirby JA (1997). A comparison of the antigen-presenting capabilities of class II MHC-expressing human lung epithelial and endothelial cells. Immunology 91, 458–463. [PubMed: 9301537]

De Calisto J, Villablanca EJ, and Mora JR (2012). FcγRI (CD64): an identity card for intestinal macrophages. Eur. J. Immunol 42, 3136–3140. [PubMed: 23255010]

De Schepper S, Verheijden S, Aguilera-Lizarraga J, Viola MF, Boesmans W, Stakenborg N, Voytyuk I, Schmidt I, Boeckx B, Dierckx de Casterlé I, et al. (2018). Self-Maintaining Gut Macrophages Are Essential for Intestinal Homeostasis. Cell 175, 400–415. [PubMed: 30173915]

Dimitriadou V, Mécheri S, Koutsilieris M, Fraser W, Al-Daccak R, and Mourad W (1998). Expression of functional major histocompatibility complex class II molecules on HMC-1 human mast cells. J. Leukoc. Biol 64, 791–799. [PubMed: 9850162]

Dotan I, Allez M, Nakazawa A, Brimnes J, Schulder-Katz M, and Mayer L (2007). Intestinal epithelial cells from inflammatory bowel disease patients preferentially stimulate $CD4^+$ T cells to proliferate and secrete interferon-gamma. Am. J. Physiol. Gastrointest. Liver Physiol 292, G1630–G1640. [PubMed: 17347451]

Ekiz HA, Conley CJ, Stephens WZ, and O'Connell RM (2020). CIPR: a web-based R/shiny app and R package to annotate cell clusters in single cell RNA sequencing experiments. BMC Bioinformatics 21, 191. [PubMed: 32414321]

Framson PE, Cho DH, Lee LY, and Hershberg RM (1999). Polarized expression and function of the costimulatory molecule CD58 on human intestinal epithelial cells. Gastroenterology 116, 1054–1062. [PubMed: 10220497]

Furusawa Y, Obata Y, Fukuda S, Endo TA, Nakato G, Takahashi D, Nakanishi Y, Uetake C, Kato K, Kato T, et al. (2013). Commensal microbe-derived butyrate induces the differentiation of colonic regulatory T cells. Nature 504, 446–450. [PubMed: 24226770]

Goodyear AW, Kumar A, Dow S, and Ryan EP (2014). Optimization of murine small intestine leukocyte isolation for global immune phenotype analysis. J. Immunol. Methods 405, 97–108. [PubMed: 24508527]

Goto Y, Panea C, Nakato G, Cebula A, Lee C, Diez MG, Laufer TM, Ignatowicz L, and Ivanov II (2014). Segmented filamentous bacteria antigens presented by intestinal dendritic cells drive mucosal Th17 cell differentiation. Immunity 40, 594–607. [PubMed: 24684957]

Gupta NT, Vander Heiden JA, Uduman M, Gadala-Maria D, Yaari G, and Kleinstein SH (2015). Change-O: a toolkit for analyzing large-scale B cell immunoglobulin repertoire sequencing data. Bioinformatics 31, 3356–3358. [PubMed: 26069265]

Author Manuscript Author Manuscript Author Manuscript Author Manuscript

Hashimoto K, Joshi SK, and Koni PA (2002).A conditional null allele of the major histocompatibility IA-beta chain gene. Genesis 32, 152–153. [PubMed: 11857806]

Hepworth MR, Monticelli LA, Fung TC, Ziegler CG, Grunberg S, Sinha R, Mantegazza AR, Ma HL, Crawford A, Angelosanto JM, et al. (2013). Innate lymphoid cells regulate $CD4^+$ T-cell responses to intestinal commensal bacteria. Nature 498, 113–117. [PubMed: 23698371]

Hershberg RM, and Mayer LF (2000). Antigen processing and presentation by intestinal epithelial cells - polarity and complexity. Immunol. Today 21, 123–128. [PubMed: 10689299]

Hershberg RM, Cho DH, Youakim A, Bradley MB, Lee JS, Framson PE, and Nepom GT (1998). Highly polarized HLA class II antigen processing and presentation by human intestinal epithelial cells. J. Clin. Invest 102, 792–803. [PubMed: 9710448]

Hughes A, Bloch KJ, Bhan AK, Gillen D, Giovino VC, and Harmatz PR (1991). Expression of MHC class II (Ia) antigen by the neonatal enterocyte: the effect of treatment with interferon-gamma. Immunology 72, 491–496. [PubMed: 1903764]

Hundorfean G, Zimmer K-P, Strobel S, Gebert A, Ludwig D, and Büning J (2007). Luminal antigens access late endosomes of intestinal epithelial cells enriched in MHC I and MHC II molecules: in vivo study in Crohn's ileitis. Am. J. Physiol. Gastrointest. Liver Physiol 293, G798–G808. [PubMed: 17673546]

Iliev ID, Mileti E, Matteoli G, Chieppa M, and Rescigno M (2009). Intestinal epithelial cells promote colitis-protective regulatory T-cell differentiation through dendritic cell conditioning. Mucosal Immunol. 2, 340–350. [PubMed: 19387433]

Jamwal DR, Laubitz D, Harrison CA, Figliuolo da Paz V, Cox CM, Wong R, Midura-Kiela M, Gurney MA, Besselsen DG, Setty P, et al. (2020). Intestinal Epithelial Expression of MHCII Determines Severity of Chemical, T-Cell-Induced, and Infectious Colitis in Mice. Gastroenterology 159, 1342–1356.e6. [PubMed: 32589883]

Joeris T, Müller-Luda K, Agace WW, and Mowat AM (2017). Diversity and functions of intestinal mononuclear phagocytes. Mucosal Immunol. 10, 845–864. [PubMed: 28378807]

Kambayashi T, and Laufer TM (2014). Atypical MHC class II-expressing antigen-presenting cells: can anything replace a dendritic cell? Nat. Rev. Immunol 14, 719–730. [PubMed: 25324123]

Karlsson M, Lundin S, Dahlgren U, Kahu H, Pettersson I, and Telemo E (2001). "Tolerosomes" are produced by intestinal epithelial cells. Eur. J. Immunol 31, 2892–2900. [PubMed: 11592064]

Kawamoto S, Maruya M, Kato LM, Suda W, Atarashi K, Doi Y, Tsutsui Y, Qin H, Honda K, Okada T, et al. (2014). Foxp3($^+$) T cells regulate immunoglobulin a selection and facilitate diversification of bacterial species responsible for immune homeostasis. Immunity 41, 152–165. [PubMed: 25017466]

Khan AA, Yurkovetskiy L, O'Grady K, Pickard JM, de Pooter R, Antonopoulos DA, Golovkina T, and Chervonsky A (2019). Polymorphic Immune Mechanisms Regulate Commensal Repertoire. Cell Rep. 29, 541–550. [PubMed: 31618625]

Kim D, Pertea G, Trapnell C, Pimentel H, Kelley R, and Salzberg SL (2013). TopHat2: accurate alignment of transcriptomes in the presence of insertions, deletions and gene fusions. Genome Biol. 14, R36. [PubMed: 23618408]

Koyama M, Mukhopadhyay P, Schuster IS, Henden AS, Hülsdünker J, Varelias A, Vetizou M, Kuns RD, Robb RJ, Zhang P, et al. (2019). MHC Class II Antigen Presentation by the Intestinal Epithelium Initiates Graft-versus-Host Disease and Is Influenced by the Microbiota. Immunity 51, 885–898.e7. [PubMed: 31542340]

Kozich JJ, Westcott SL, Baxter NT, Highlander SK, and Schloss PD (2013). Development of a dual-index sequencing strategy and curation pipeline for analyzing amplicon sequence data on the MiSeq Illumina sequencing platform. Appl. Environ. Microbiol 79, 5112–5120. [PubMed: 23793624]

Kubinak JL, Petersen C, Stephens WZ, Soto R, Bake E, O'Connell RM, and Round JL (2015a). MyD88 signaling in T cells directs IgA-mediated control of the microbiota to promote health. Cell Host Microbe 17, 153–163. [PubMed: 25620548]

Kubinak JL, Stephens WZ, Soto R, Petersen C, Chiaro T, Gogokhia L, Bell R, Ajami NJ, Petrosino JF, Morrison L, et al. (2015b). MHC variation sculpts individualized microbial communities that control susceptibility to enteric infection. Nat. Commun 6, 8642. [PubMed: 26494419]

Author Manuscript Author Manuscript Author Manuscript Author Manuscript

Lathrop SK, Bloom SM, Rao SM, Nutsch K, Lio CW, Santacruz N, Peterson DA, Stappenbeck TS, and Hsieh CS (2011). Peripheral education of the immune system by colonic commensal microbiota. Nature 478, 250–254. [PubMed: 21937990]

Lawrence M, Huber W, Pagès H, Aboyoun P, Carlson M, Gentleman R, Morgan MT, and Carey VJ (2013). Software for computing and annotating genomic ranges. PLoS Comput. Biol 9, e1003118. [PubMed: 23950696]

Lord SJ, Velle KB, Mullins RD, and Fritz-Laylin LK (2020). SuperPlots: Communicating reproducibility and variability in cell biology. J. Cell Biol 219, e202001064. [PubMed: 32346721]

Madison BB, Dunbar L, Qiao XT, Braunstein K, Braunstein E, and Gumucio DL (2002). Cis elements of the villin gene control expression in restricted domains of the vertical (crypt) and horizontal (duodenum, cecum) axes of the intestine. J. Biol. Chem 277, 33275–33283. [PubMed: 12065599]

Maggio-Price L, Seamons A, Bielefeldt-Ohmann H, Zeng W, Brabb T, Ware C, Lei M, and Hershberg RM (2013). Lineage targeted MHC-II transgenic mice demonstrate the role of dendritic cells in bacterial-driven colitis. Inflamm. Bowel Dis. 19, 174–184.

Mandal S, Van Treuren W, White RA, Eggesbø M, Knight R, and Peddada SD (2015). Analysis of composition of microbiomes: a novel method for studying microbial composition. Microb. Ecol. Health Dis 26, 27663. [PubMed: 26028277]

Martin M (2011). Cutadapt removes adapter sequences from high-throughput sequencing reads. EMBnet. J 17, 1.

Mazzini E, Massimiliano L, Penna G, and Rescigno M (2014). Oral tolerance can be established via gap junction transfer of fed antigens from $CX3CR1^{+}$ macrophages to $CD103^{+}$ dendritic cells. Immunity 40, 248–261. [PubMed: 24462723]

Melo-Gonzalez F, Kammoun H, Evren E, Dutton EE, Papadopoulou M, Bradford BM, Tanes C, Fardus-Reid F, Swann JR, Bittinger K, et al. (2019). Antigen-presenting ILC3 regulate T cell-dependent IgA responses to colonic mucosal bacteria. J. Exp. Med 216, 728–742. [PubMed: 30814299]

Miyake K, Shiozawa N, Nagao T, Yoshikawa S, Yamanishi Y, and Karasuyama H (2017).Trogocytosis of peptide-MHC class II complexes from dendritic cells confers antigen-presenting ability on basophils. Proc. Natl. Acad. Sci. USA 114, 1111–1116. [PubMed: 28096423]

Murai M, Turovskaya O, Kim G, Madan R, Karp CL, Cheroutre H, and Kronenberg M (2009). Interleukin 10 acts on regulatory T cells to maintain expression of the transcription factor Foxp3 and suppressive function in mice with colitis. Nat. Immunol 10, 1178–1184. [PubMed: 19783988]

Muzumdar MD, Tasic B, Miyamichi K, Li L, and Luo L (2007). A global double-fluorescent Cre reporter mouse. Genesis 45, 593–605. [PubMed: 17868096]

Niess JH, Brand S, Gu X, Landsman L, Jung S, McCormick BA, Vyas JM, Boes M, Ploegh HL, Fox JG, Littman DR, and Reinecker H-C (2005). CX3CR1-mediated dendritic cell access to the intestinal lumen and bacterial clearance. Science 307, 254–258. [PubMed: 15653504]

Oksanen J, Blanchet FG, Friendly M, Kindt R, Legendre P, McGlinn D, Minchin PR, O'Hara RB, Simpson GL, Solymos P, Stevens MHH, Szoecs E, and Wagner H (2019). vegan: Community Ecology Package.

Oliphant CJ, Hwang YY, Walker JA, Salimi M, Wong SH, Brewer JM, Englezakis A, Barlow JL, Hams E, Scanlon ST, et al. (2014). MHCII-mediated dialog between group 2 innate lymphoid cells and CD4(+) T cells potentiates type 2 immunity and promotes parasitic helminth expulsion. Immunity 41, 283–295. [PubMed: 25088770]

Östman S, Taube M, and Telemo E (2005). Tolerosome-induced oral tolerance is MHC dependent. Immunology 116, 464–476. [PubMed: 16313360]

Pabst O (2013). Trafficking of regulatory T cells in the intestinal immune system. Int. Immunol 25, 139–143. [PubMed: 23257631]

Pedregosa F, Varoquaux G, Gramfort A, Michel V, Thirion B, Grisel O, Blondel M, Prettenhofer P, Weiss R, Dubourg V, et al. (2011). Scikit-learn: Machine learning in Python. J. Mach. Learn. Res 12, 2825–2830.

Ritchie ME, Phipson B, Wu D, Hu Y, Law CW, Shi W, and Smyth GK (2015). limma powers differential expression analyses for RNA-sequencing and microarray studies. Nucleic Acids Res. 43, e47. [PubMed: 25605792]

Author Manuscript Author Manuscript Author Manuscript Author Manuscript

Rognes T, Flouri T, Nichols B, Quince C, and Mahé F (2016). VSEARCH: a versatile open source tool for metagenomics. PeerJ 4, e2584. [PubMed: 27781170]

Rogoz A, Reis BS, Karssemeijer RA, and Mucida D (2015). A 3-D enteroid-based model to study T-cell and epithelial cell interaction. J. Immunol. Methods 421, 89–95. [PubMed: 25841547]

Sefik E, Geva-Zatorsky N, Oh S, Konnikova L, Zemmour D, McGuirem Abigail Manson Burzyn D, Ortiz-Lopez A, Lobera M, Yang J, Ghosh S, Earl A, Snapper SB, Jupp R, Kasper D, Mathis D, and Benoist C (2015). Individual intestinal symbionts induce a distinct population of RORγndividual intestinal. Science 349, 993–997. [PubMed: 26272906]

Shaw TN, Houston SA, Wemyss K, Bridgeman HM, Barbera TA, Zangerle-Murray T, Strangward P, Ridley AJL, Wang P, Tamoutounour S, et al. (2018). Tissue-resident macrophages in the intestine are long lived and defined by Tim-4 and CD4 expression. J. Exp. Med 215, 1507–1518. [PubMed: 29789388]

Shi HZ, Humbles A, Gerard C, Jin Z, and Weller PF (2000). Lymph node trafficking and antigen presentation by endobronchial eosinophils. J. Clin. Invest 105, 945–953. [PubMed: 10749574]

Silverman M, Kua L, Tanca A, Pala M, Palomba A, Tanes C, Bittinger K, Uzzau S, Benoist C, and Mathis D (2017). Protective major histocompatibility complex allele prevents type 1 diabetes by shaping the intestinal microbiota early in ontogeny. Proc. Natl. Acad. Sci. USA 114, 9671–9676. [PubMed: 28831005]

Sokol CL, Chu NQ, Yu S, Nish SA, Laufer TM, and Medzhitov R (2009). Basophils function as antigen-presenting cells for an allergen-induced T helper type 2 response. Nat. Immunol 10, 713–720. [PubMed: 19465907]

Sujino T, London M, Hoytema van Konijnenburg DP, Rendon T, Buch T, Silva HM, Lafaille JJ, Reis BS, and Mucida D (2016). Tissue adaptation of regulatory and intraepithelial $CD4^+$ T cells controls gut inflammation. Science 352, 1581–1586. [PubMed: 27256884]

Sun C-M, Hall JA, Blank RB, Bouladoux N, Oukka M, Mora JR, and Belkaid Y (2007). Small intestine lamina propria dendritic cells promote de novo generation of Foxp3 T reg cells via retinoic acid. J. Exp. Med 204, 1775–1785. [PubMed: 17620362]

Takahashi S, Tomita J, Nishioka K, Hisada T, and Nishijima M (2014). Development of a prokaryotic universal primer for simultaneous analysis of Bacteria and Archaea using next-generation sequencing. PLoS ONE 9, e105592. [PubMed: 25144201]

Thelemann C, Eren RO, Coutaz M, Brasseit J, Bouzourene H, Rosa M, Duval A, Lavanchy C, Mack V, Mueller C, et al. (2014). Interferon-γ induces expression of MHC class II on intestinal epithelial cells and protects mice from colitis. PLoS ONE 9, e86844. [PubMed: 24489792]

Thornton AM, Korty PE, Tran DQ, Wohlfert EA, Murray PE, Belkaid Y, and Shevach EM (2010). Expression of Helios, an Ikaros transcription factor family member, differentiates thymic-derived from peripherally induced $Foxp3^+$ T regulatory cells. J. Immunol 184, 3433–3441. [PubMed: 20181882]

Torre D, Lachmann A, and Ma'ayan A (2018). BioJupies: Automated Generation of Interactive Notebooks for RNA-Seq Data Analysis in the Cloud. Cell Syst. 7, 556–561. [PubMed: 30447998]

Umesaki Y, Okada Y, Matsumoto S, Imaoka A, and Setoyama H (1995). Segmented filamentous bacteria are indigenous intestinal bacteria that activate intraepithelial lymphocytes and induce MHC class II molecules and fucosyl asialo GM1 glycolipids on the small intestinal epithelial cells in the ex-germ-free mouse. Microbiol. Immunol 39, 555–562. [PubMed: 7494493]

Van Niel G, Mallegol J, Bevilacqua C, Candalh C, Brugière S, Tomaskovic-Crook E, Heath JK, Cerf-Bensussan N, and Heyman M (2003). Intestinal epithelial exosomes carry MHC class II/peptides able to inform the immune system in mice. Gut 52, 1690–1697. [PubMed: 14633944]

Vidal K, Grosjean I, evillard JP, Gespach C, and Kaiserlian D (1993). Immortalization of mouse intestinal epithelial cells by the SV40-large T gene. Phenotypic and immune characterization of the MODE-K cell line. J. Immunol. Methods 166, 63–73. [PubMed: 7693823]

Westendorf AM, Fleissner D, Groebe L, Jung S, Gruber AD, Hansen W, and Buer J (2009). $CD4^+Foxp3^+$ regulatory T cell expansion induced by antigen-driven interaction with intestinal epithelial cells independent of local dendritic cells. Gut 58, 211–219. [PubMed: 18832523]

Author Manuscript Author Manuscript Author Manuscript Author Manuscript

Wosen JE, Mukhopadhyay D, Macaubas C, and Mellins ED (2018). Epithelial MHC Class II Expression and Its Role in Antigen Presentation in the Gastrointestinal and Respiratory Tracts. Front. Immunol 9, 2144. [PubMed: 30319613]

Author Manuscript Author Manuscript Author Manuscript Author Manuscript

Highlights

- MHC class II is highly expressed on ileal intestinal epithelial cells (IECs)
- Lack of IEC-MHC class II results in reduced immune and microbiota constraint
- MHC class II can be transferred from IECs to gut mononuclear phagocytes

Author Manuscript Author Manuscript Author Manuscript Author Manuscript

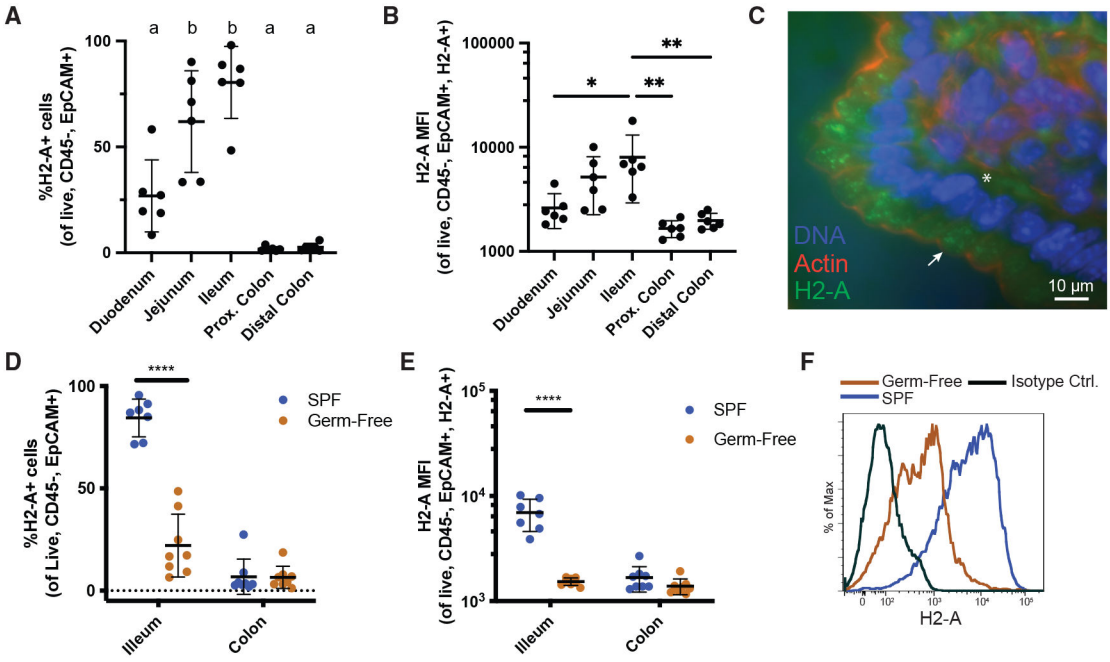

Figure 1. MHC class II is differentially expressed on epithelia along the murine intestinal tract and inducible by the microbiota

(A and B) The percentage positive (A) and expression level (B) (MFI, median fluorescent intensity) of the H2-A protein on IECs of SPF-raised C57BL/6 mice. n = 6 mice, a single experiment representative of three independent experiments is shown. Letters denote significance between groups. Ordinary one-way ANOVA with Tukey's multiple comparison correction was used.

(C) Representative cryosection immunohistochemistry image of a WT ileal villus illustrating intense apical granular cytoplasmic staining (arrow) of H2-A on IECs, and diffuse basolateral surface H2-A on IECs (asterisk).

(D and E) The percentage positive (D) and MFI (E) of H2-A on GF and SPF male Swiss-Webster mice. n = 7–8 mice per group. An unpaired Student's t test was used, ****p < 0.0001.

(F) A representative histogram of H2-A staining from the ileum shows very low H2-A on GF mice is present above the isotype control background signal.

Author Manuscript Author Manuscript Author Manuscript Author Manuscript

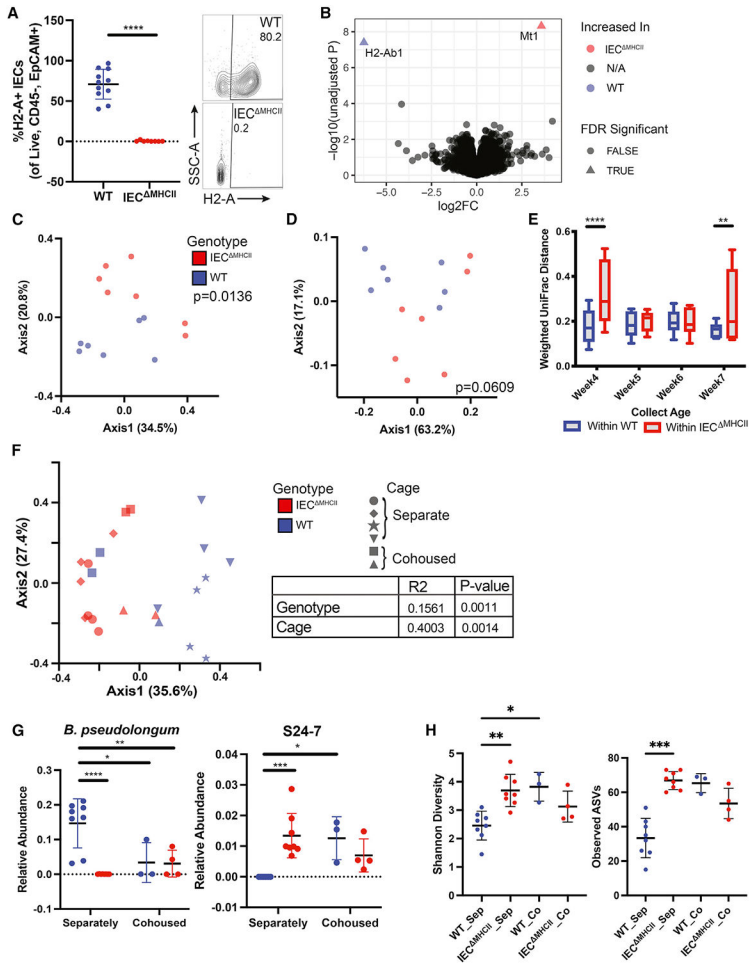

Figure 2. Lack of IEC-intrinsic MHC class II has no effect on the epithelial transcriptome but controls the variability of microbial communities

(A) Ileum-derived IECs stained for H2-A show knockout of H2-A on IECs in IEC$^{\Delta MHCII}$ mice. n = 11 WT and n = 8 IEC$^{\Delta MHCII}$. A Student's t test was used.

(B) Volcano plot of RNA expression levels from sorted ileal IECs shows that only the targeted gene (*H2-Ab1*) is significantly changed (after FDR correction; 13,481 genes tested) in IEC$^{\Delta MHCII}$ mice. The increased *Mt1* is an artifact that reflects Cre expression, due to a small fragment of this gene left on the *Villin*:Cre expression construct.

(C and D) Principal coordinates plots from Bray-Curtis (C) or weighted-UniFrac (D) metrics of fecal microbiota from mice housed by genotype (2 cages per genotype, 3–4 mice per cage). Permanova p values are shown with 9,999 permutations.

(E) Weighted-UniFrac distances from fecal microbiota of male mice individually housed post-weaning. n = 6WT and 5 IEC$^{\Delta MHCII}$, except at week 5 when only 3WT samples had enough quality sequences for analysis. Two-way ANOVA with Holm-Sidak multiple testing correction was used.

(F) Principal coordinates plot of ileal microbiota from Bray-Curtis distances along with Anosim results with cage and genotype factors as the independent variables.

(G) Relative abundance of 2 taxa significantly different between genotypes in the ileum when separately housed. Both taxa initially identified with ANCOM (see main text) at

Author Manuscript Author Manuscript Author Manuscript Author Manuscript

the level of ASVs (2 each) were plotted as means of the ASVs summarized to their best taxonomic classification with significance between groups on plots shown with two-way ANOVA with Tukey's correction for multiple testing.
(H) Ileal microbiota alpha-diversity metrics. A Kruskal-Wallis test with Dunn's correction was used.

Author Manuscript Author Manuscript Author Manuscript Author Manuscript

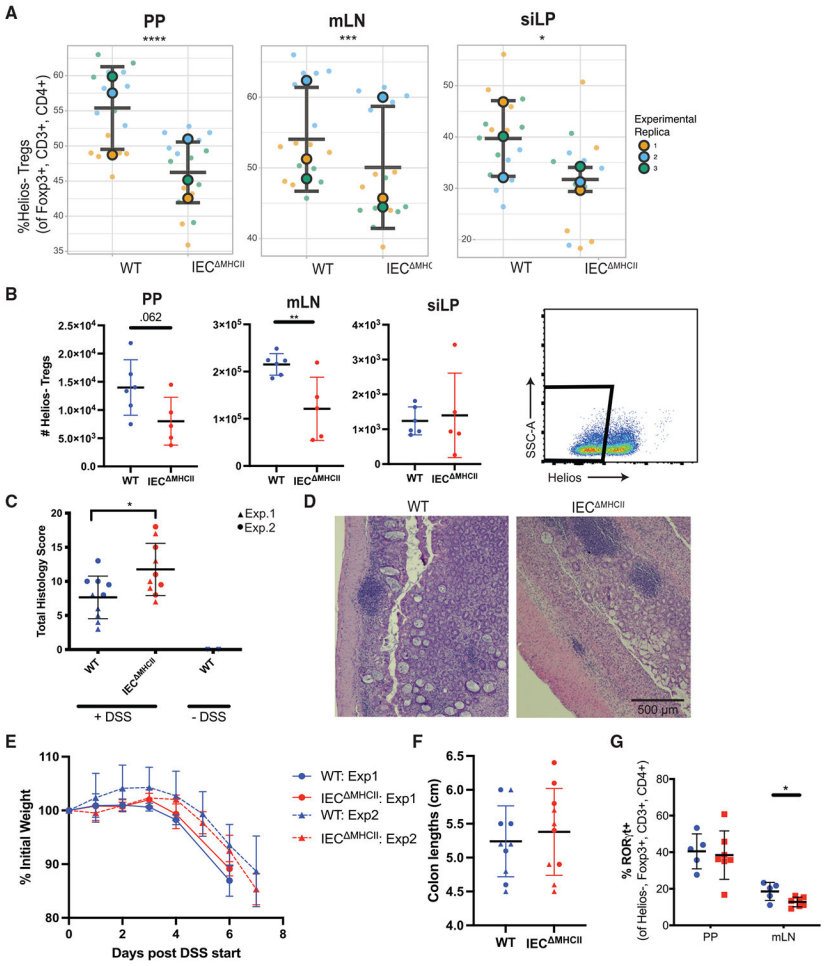

Figure 3. Lack of IEC-derived MHC class II results in reduced microbiota-responsive Tregs and increased susceptibility to colitis

(A) The proportion of Helios$^-$ Tregs (CD3$^+$, CD4$^+$, Foxp3$^+$) in 9- to 12-week-old female mice under homeostatic conditions. Data are represented as SuperPlots showing three experimental replicates. Bars are mean and SD among experimental replicates. Stars indicate genotype significance using a 2-way ANOVA with experiment and genotype as main effects (see Table S2 for a full ANOVA table).

(B) Absolute numbers of Helios$^-$ Tregs from one experiment. An unpaired t test was used. A representative flow plot of Helios gating from mLN Tregs was used.

(C) Histology scores from DSS-treated mice. Combined data from two experiments, indicated by shape, are shown. n = 10 WT and n = 10 IEC$^{\Delta MHCII}$. An unpaired t test with Welch's correction was used. Untreated WT slide scores were included as control but not statistically tested.

(D) Representative images of H&E-stained sections from DSS experiments.

(E and F) Weight loss (E) and colon lengths (F) from 2 DSS experiments.

(G) RORγt$^+$ Tregs in Peyer's patches and mLN. Data are representative of 4 experiments, among which decreases in PP RORγt$^+$ Tregs are sometimes observed. A Student's t test with Holm-Sidak's multiple testing correction was used.

Author Manuscript
Author Manuscript
Author Manuscript
Author Manuscript

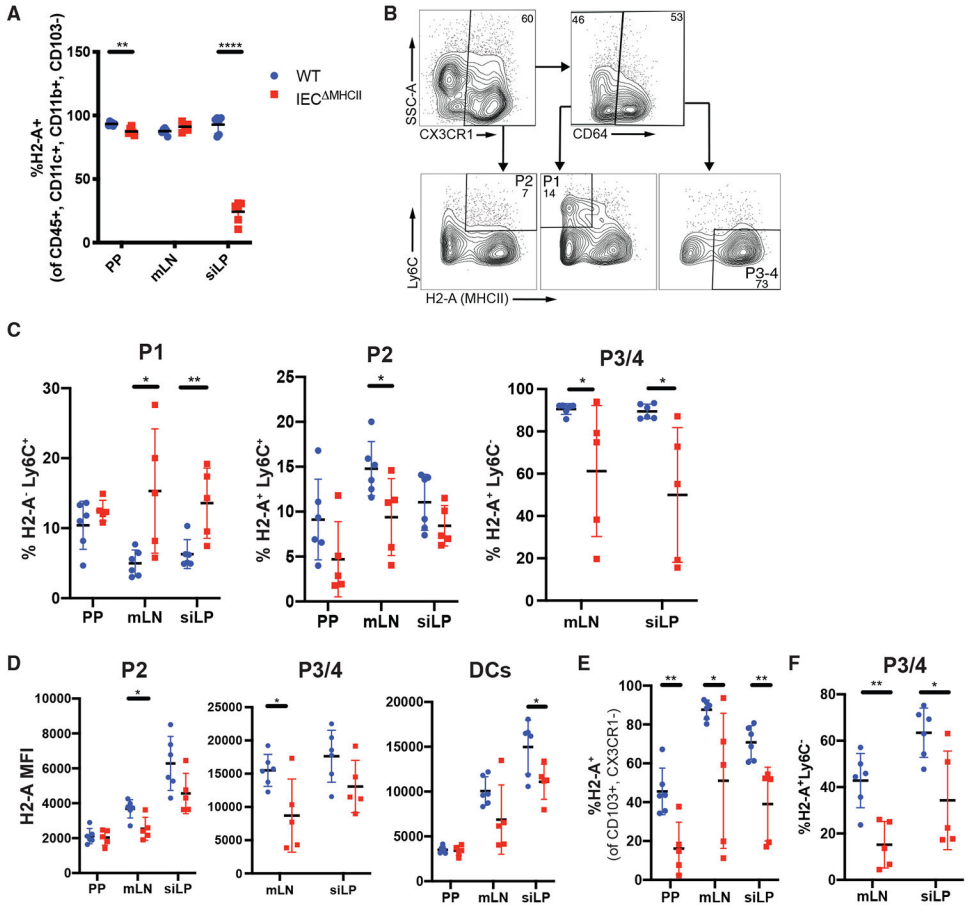

Figure 4. IEC intrinsic H2-A influences H2-A levels on MNP cells

(A) The initial observation of the proportion of H2-A$^+$ cells among immune cells with broad myeloid markers. One experiment; a Student's t test with Holm-Sidak's multiple testing correction was used.

(B) Representative flow plots illustrate the gating strategy used to identify P1–4 monocyte/macrophage cells. CD45$^+$, Lin$^-$ (CD3, NK1.1, Siglec-F, CD19), CD11b$^+$, CD11c$^+$ cells are input.

(C–E) Proportion (C and E) and MFI (D) of P1, P2, and P3/4 monocyte/macrophages (C and D) and DCs (D and E) under homeostatic SPF conditions in 9-week-old male and female mice. P3/4 are not shown for PP because they are not CD64$^+$. n = 6 WT and 5 IEC$^{\Delta MHCII}$. Data are representative of 2 experiments. A Student's t test with Holm-Sidak's multiple testing correction was used.

(F) As in (C)–(E) but showing the CD11c-negative subset of P3/4 macrophages.

Author Manuscript Author Manuscript Author Manuscript Author Manuscript

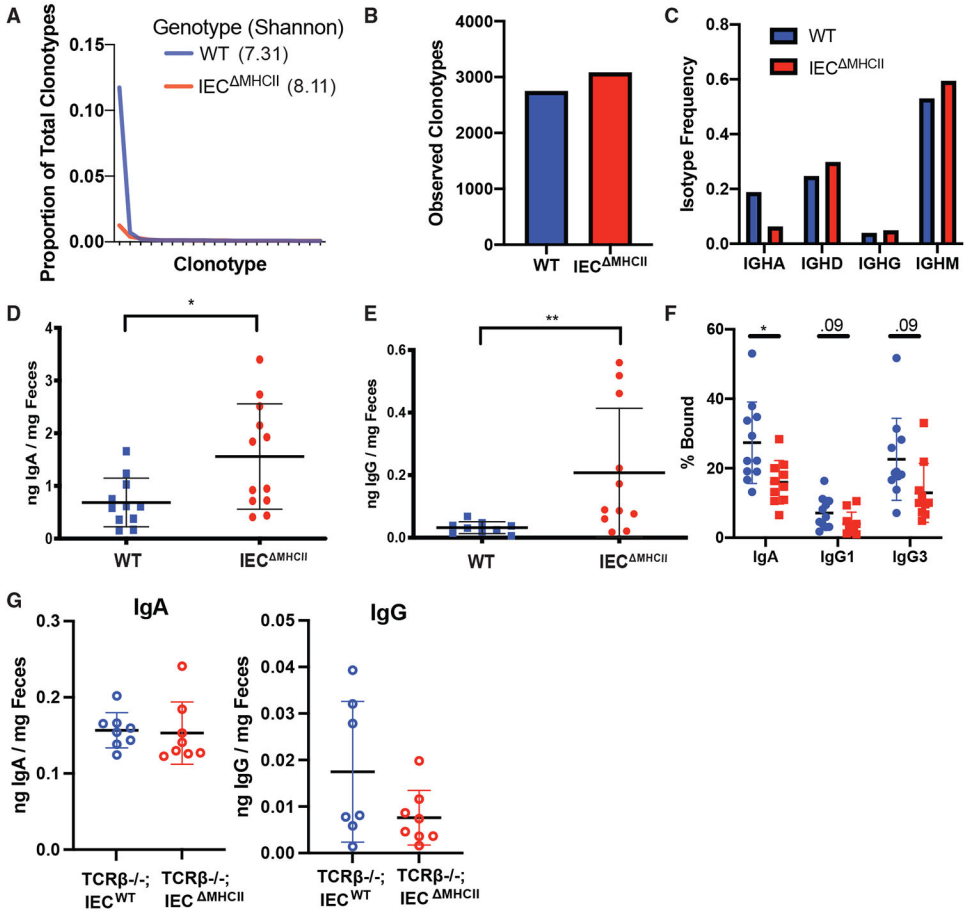

Figure 5. MHC class II constrains immune responses toward intestinal microbes

(A and B) The distribution (A) and total number (B) of Ig clonotypes detected in PP scRNA-seq data. The rank-abundance curve (A) shows only the top 20 clonotypes along with the Shannon diversity indices for each genotype, which takes into account the total number and distribution of clonotypes. Clonotype analysis was performed after subsampling without replacement to 3,215 observations in each group. Data are from one scRNA-seq experiment with an equivalent number of cells pooled from 4 WT or 4 IEC$^{\Delta MHCII}$ mice.

(C) Ig heavy-chain isotype frequency in PP from scRNA-seq data.

(D and E) Total fecal IgA and IgG quantified by ELISA, normalized to fecal weight. n = 11–12 mice. Data are representative of 2 experiments. A t test with Welch's correction was used.

(F) The proportion of bacterial cells (SYBR^{+}) from feces that are bound by immunoglobulins. Data are representative of 2 experiments. t tests with Holm-Sidak's multiple testing correction were used.

(G) Total fecal IgA and IgG are not different in T cell-deficient mice. n = 8 in both groups. A t test with Welch's correction was used.

Author Manuscript Author Manuscript Author Manuscript Author Manuscript

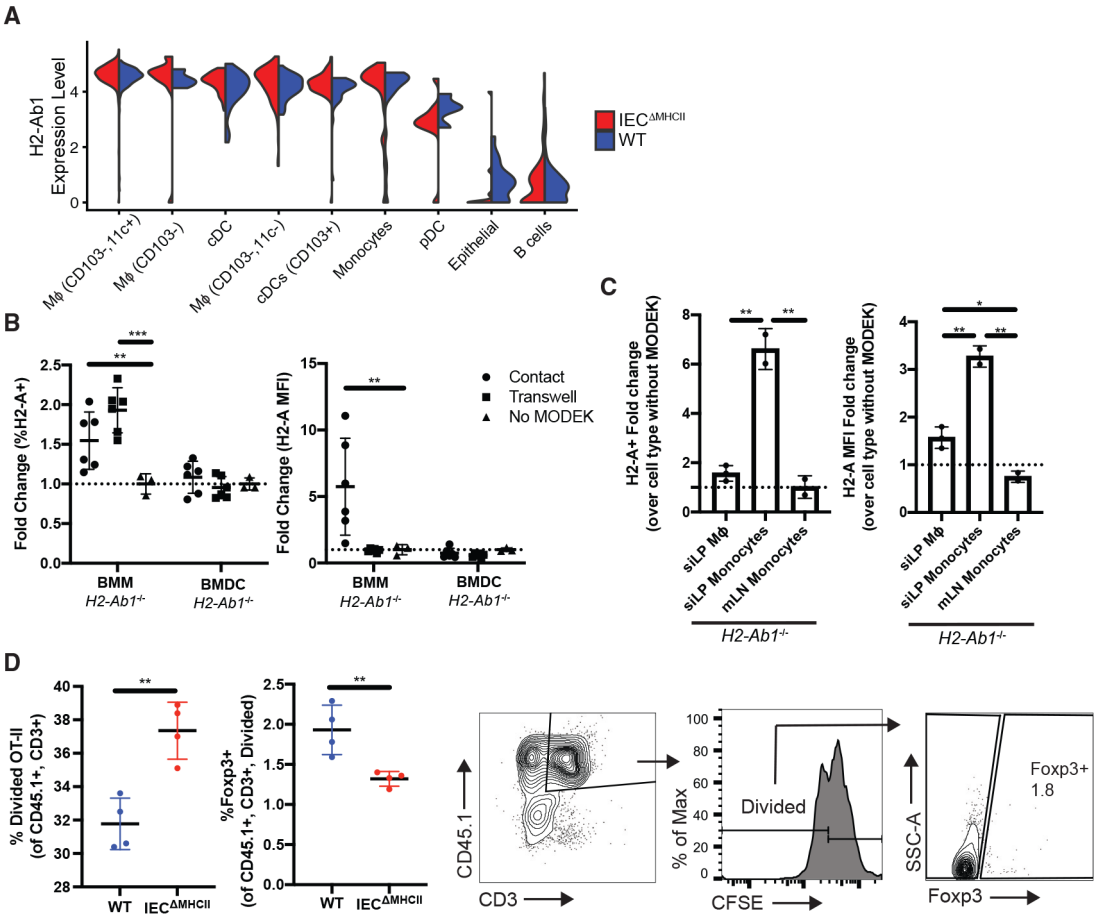

Figure 6. MNPs can acquire H2-A from IECs to induce T cell responses

(A) Violin plots of *H2-Ab1* transcripts from scRNA-seq data in the siLP show knockout of *H2-Ab1* in IECs but normal expression in other known MHC class II^{+} cells types.

(B) Results from *in vitro* association of MODEK (H2^{k} haplotype) cells and *H2-Ab1*$^{-/-}$ C57BL/6 bone-marrow-derived MNPs. Data are expressed as a fold change of H2-A^{k} signal over the background from the average of MNPs incubated without MODEK cells. Two-way ANOVA with Holm-Sidak's multiple comparison test within cell type to no MODEK control was used.

(C) As in (B) (quantifying H2-A^{k}) but using MNPs sorted directly from the tissue of *H2-Ab1*$^{-/-}$ C57BL/6 mice. Ordinary one-way ANOVA with Tukey's multiple comparison test was used.

(D) The proportion of CFSE-labeled OT-II cells that underwent 1 or more divisions and were Foxp3^{+} after incubating with OVA-pulsed macrophages sorted directly from the tissue of WT or IEC$^{\Delta MHCII}$ mice. Representative flow plots illustrate the gating strategy for assessing proliferating OT-II cells. Data are representative of 2 experiments; a Student's t test was used.

Author Manuscript Author Manuscript Author Manuscript Author Manuscript

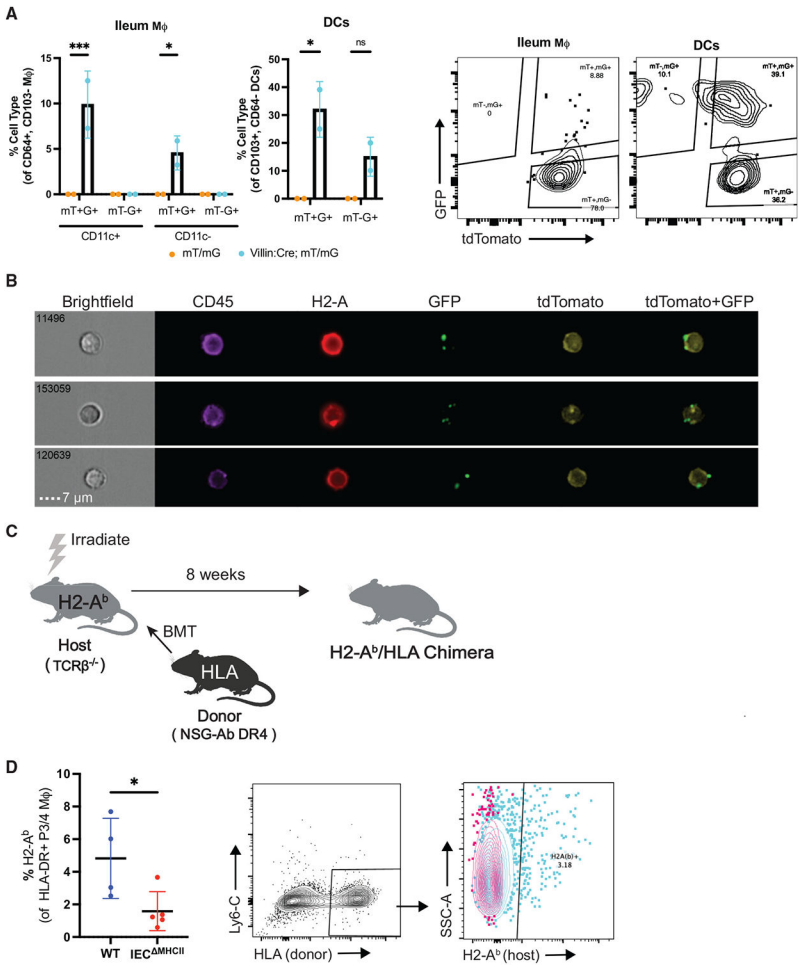

Figure 7. MNPs can acquire MHC class II from IECs *in vivo*

(A) The proportion of $mT^{+}mG^{+}$ MNP subsets in the siLP. Cells subsets are pregated on Live, $Dump^{-}$ (CD3, CD19, NK1.1, Ly6G), $CD45^{+}$, and MHC class II^{+}. Representative flow plots are shown for $CD11c^{+}$ macrophages and DCs. Two-way ANOVA with Holm-Sidak correction was used.

(B) Representative image panel of cells from imaging flow cytometry analysis of $mT^{+}mG^{+}$ MNPs. Cells are Live, $Dump^{-}$ (CD3, IgM), $CD45^{+}$, and MHC class II^{+}. No CD11c or CD11b subsetting due to reduced channel availability on imaging cytometry platform was used.

(C) A cartoon schematic of mixed MHC class II bone-marrow transfer experiments.

(D) The percentage of host MHC class II ($H2\text{-}A^{b}$) positive donor cells (HLA-DR) in the siLP. Cells are $CD11c^{-}$ P3/P4 macrophages gated as in previous figures. A representative plot (pregated on $CD45^{+}$, Dump-, $CD11b^{+}/CD11c^{+}$, and $CX3CR1^{+}/CD64^{+}$ cells) is shown, along with an overlay of the $H2\text{-}A^{b}$ isotype control demonstrating the MHC class II-haplotype specificity of the staining.

Author Manuscript Author Manuscript Author Manuscript Author Manuscript

KEY RESOURCES TABLE

Reagent or resource	Source	Identifier
Antibodies		
CD4 FITC, clone RM4-5	Biolegend	Cat#100510; RRID: AB_312713
Foxp3 APC, clone FJK-16S	ThermoFisher Scientific	Cat#17-5773-82; RRID: AB_469457
Helios PerCP-Cy5.5, clone 22F6	Biolegend	Cat#137230; RRID: AB_2561640
RORγt eFluor610, clone B2D	ThermoFisher Scientific	Cat#61-6981-82; RRID: AB_2574650
CD3 violetFluor 450, clone 17A2	Tonbo Biosciences	Cat#75-0032; RRID: AB_2621923
CD3e APC Cy7, clone 145-2C11	Biolegend	Cat#100330, RRID: AB_1877170
CD3e Pacific Blue, clone 145-2C11	Biolegend	Cat#100334; RRID: AB_2028475
CD3e PerCP-Cy5.5, clone 145-2C11	Tonbo Biosciences	Cat#65-0031; RRID:AB_2621872
IFNγ PE, clone XMG1.2	Biolegend	Cat#505808; RRID: AB_315402
IL-17A PE-Cy7, clone eBio17B7	ThermoFisher Scientific	Cat#25-7177-82; RRID: AB_10732356
EpCAM APC, clone G8.8	ThermoFisher Scientific	Cat#17-5791-82; RRID: AB_2716944
EpCAM eFluor450, clone G8.8	ThermoFisher Scientific	Cat#48-5791-80; RRID: AB_10717391
CD45 violetFluor 450, clone 30-F11	Tonbo Biosciences	Cat#75-0451; RRID: AB_2621947
CD45 PE-Cy7, clone 30-F11	Tonbo Biosciences	Cat#60-0451; RRID: AB_2621848
CD45 PE, clone 30-F11	Tonbo Biosciences	Cat#50-0451; RRID: AB_2621763
CD103 PE, clone 2E7	Biolegend	Cat#121406; RRID: AB_1133989
CD103 APC-Cy7, clone 2E7	Biolegend	Cat#121432; RRID: AB_2566552
CD11c SuperBright 600, clone N418	ThermoFisher Scientific	Cat#63-0114-82; RRID: AB_2722930
CD11c FITC, clone N418	Biolegend	Cat#117306, RRID: AB_313775
Anti-mouse CD16/CD32 (Fc Shield)	Tonbo Biosciences	Cat#70-0161
I-A^k PE, clone 10-3.6	Biolegend	Cat#109908; RRID: AB_313457
CX3CR1 PE/Dazzle 594, clone SA011F11	Biolegend	Cat#149013; RRID: AB_2565697
CX3CR1 Brilliant Violet 510, clone SA011F11	Biolegend	Cat#149025; RRID: AB_2565707
CD11b PE-Cy7, clone M1/70	Tonbo Biosciences	Cat#60-0112; RRID: AB_2621836
Ly-6C AlexaFluor 488, clone HK1.4	Biolegend	Cat#128022; RRID: AB_10639728
CD64 Brilliant Violet 711, clone X54-5/7.1	Biolegend	Cat#139311; RRID: AB_2563846
CD279 (PD-1) PE-Cy7, clone 29F.1A12	Biolegend	Cat#135216; RRID: AB_10689635
CD185 (CXCR5) PE, clone SPRCL5	ThermoFisher Scientific	Cat#12-7185-80; RRID: AB_11218887
CD45.1 FITC, clone A20	Biolegend	Cat#110705; RRID: AB_313494
CD45.1 PE, clone A20	Tonbo Biosciences	Cat#50-0453; RRID: AB_2621765
CD4 violetFluor 450, clone GK1.5	Tonbo Biosciences	Cat#75-0041; RRID: AB_2621927
CD45.2 PE-Cy7, clone 104	Tonbo Biosciences	Cat#60-0454; RRID: AB_2621851
I-A/I-E (H2-A) PE, clone M5/114.15.2	Biolegend	Cat#107608; RRID: AB_313323
I-A/I-E (H2-A) APC, clone M5/114.15.2	Biolegend	Cat#107613; RRID: AB_313328
I-A/I-E (H2-A) AlexaFluor 647, clone M5/114.15.2	Biolegend	Cat#107618; RRID: AB_493525
I-Ab (H2-A^b) APC, clone AF6-120.1	Biolegend	Cat#116418; RRID: AB_10574160
HLA-DR PE, clone L243	Tonbo Biosciences	Cat#50-9952; RRID: AB_2621813
CD19 PerCP-Cy5.5, clone 1D3	Tonbo Biosciences	Cat#65-0193; RRID: AB_2621887
Ly-6G PerCP-Cy5.5, clone 1A8	Tonbo Biosciences	Cat#65-1276; RRID: AB_2621899

Author Manuscript Author Manuscript Author Manuscript Author Manuscript

Reagent or resource	Source	Identifier
NK1.1 (CD161) PerCP-Cy5.5, clone PK136	Tonbo Biosciences	Cat#65-5941; RRID: AB_2621910
CD80 PE, clone 16-10A1	Biolegend	Cat#104707; RRID: AB_313128
IgA PE, clone mA-6e1	ThermoFisher Scientific	Cat#12-4204-83; RRID: AB_465918
IgG1 CruzFluor 555	Santa Cruz Biotechnology	Cat#sc-395765
IgG3 CruzFluor 555	Santa Cruz Biotechnology	Cat#sc-395780
IgM APC-Cy7, clone RMM-1	Biolegend	Cat#406516; RRID: AB_10660305
IgD AlexaFluor647, clone 11-26c.2a	Biolegend	Cat#405708; RRID: AB_893528
B220 PerCP-Cy5.5, clone RA3-6B2	ThermoFisher Scientific	Cat#45-0452-82; RRID: AB_1107006
GL7 FITC, clone GL7	Biolegend	Cat#144604; RRID: AB_2561697
FAS (CD95) PE-Cy7, clone Jo2	BD Biosciences	Cat#557653; RRID: AB_396768
Bacterial and virus strains		
Biological samples		N/A
Chemicals, peptides, and recombinant proteins		
Dextran sulfate sodium (DSS) salt, MW36000-50000	MP Bio	Cat#0216011090; CAS: 9011-18-1
Ghost Dye Red 780	Tonbo Biosciences	Cat#13-0865-T100
Ghost Dye Violet 510	Tonbo Biosciences	Cat#13-0870-T100
OVA peptide 329-337	Anaspec	Cat#AS-64777
Ovalbumin	Sigma	Cat#A5503
CFSE	ThermoFisher Scientific	Cat#50-169-50
GM-CSF	Biolegend	Cat#576304
CSF	Biolegend	Cat#574802
Recombinant mouse IFNγ (carrier-free)	Biolegend	Cat#575306
Sodium Pyruvate	Corning	Cat#10013CV
Penicillin-Streptomycin	Corning	Cat#30-001-C1
Non-essential amino acids	Corning	Cat#25-025-C1
Pam3CSK4	Invivogen	Cat#tlrl-pms
Dispase II	Millipore-Sigma	Cat#4942078001
DNase I	Worthington Biochemical	Cat#LS002139
Collagenase D	Millipore-Sigma	Cat#11088866001
SYBR Green I	ThermoFisher Scientific	Cat#S7563
FITC-dextran (3000-5000 MW)	Millipore-Sigma	Cat#FD4; CAS: 60842-46-8
TRIzol Reagent	ThermoFisher Scientific	Cat#15596026
LightCycler 480 SYBR Green I Master Mix	Roche	Cat#04707516001
Phalloidin Fluorescent Dye 555-I	Abnova	Cat#u0289
Formalin, buffered 10%	Fisher Scientific	Cat#SF100-4
Critical commercial assays		
CD45+ microbeads, mouse	Miltenyi	Cat#130-052-301
CD4+ T cell isolation kit, mouse	Miltenyi	Cat#130-104-454
Chromium Single Cell 5′ Library and Gel Bead Kit	10X Genomics	Cat#PN-1000006
Chromium Single Cell 5′ Library Construction Kit	10X Genomics	Cat#PN-1000020
Chromium Single Cell V(D)J Enrichment Kit, Mouse B Cell	10X Genomics	Cat#PN-1000072
Chromium Single Cell A Chip Kit	10X Genomics	Cat#PN-120236

Author Manuscript Author Manuscript Author Manuscript Author Manuscript

Reagent or resource	Source	Identifier
Direct-zol RNA microprep	Zymo Research	Cat#R2061
PowerFecal DNA Isolation Kit	QIAGEN	Cat#12830-50
qScript cDNA SuperMix	QuantaBio	Cat#95048
TruSeq Stranded RNA kit with Ribo-Zero Gold	Illumina	Cat#RS-122-2301
NEBNext Ultra II Directional RNA Library Prep Kit	NEB	Cat#E7760
IgG (Total) Mouse ELISA Kit	ThermoFisher Scientific	Cat#88-50400-88
IgA Mouse ELISA Kit	ThermoFisher Scientific	Cat#88-50450-22
Deposited data		
Raw 16S sequence data	This paper	SRA: SRP334816
Processed 16S sequence data and processing code	This paper	https://doi.org/10.5281/zenodo.5485145
Raw and analyzed RNaseq, sorted IECs	This paper	GEO: GSE183709
Raw and analyzed RNaseq, ileum tissue during DSS-colitis	This paper	GEO: GSE183708
Raw and analyzed scRNaseq CD45+ cell 5′ expression data	This paper	GEO: GSE183710
Raw and analyzed scRNaseq V(D)J data	This paper	GEO: GSE183711
Experimental models: Cell lines		
MODEK cells	Vidal et al., 1993	N/A
Experimental models: Organisms/strains		
Mouse: *H2-Ab1*$^{loxP/loxP}$	The Jackson Laboratory	Cat#013181
Mouse: *Villin*:Cre	The Jackson Laboratory	Cat#004586
Mouse: IEC$^{\Delta MHCII}$: *H2-Ab1*$^{loxP/loxP}$; *Villin*:Cre$^{Tg/-}$	This paper	N/A
Mouse: WT: *H2-Ab1*$^{loxP/loxP}$; *Villin*:Cre$^{-/-}$	This paper	N/A
Mouse: TCRβ$^{-/-}$	The Jackson Laboratory	Cat#002118
Mouse: *H2-Ab1*$^{-/-}$	Taconic	Cat#ABBN12
Mouse: mT/mG	The Jackson Laboratory	Cat#007676
Mouse: NSG-Ab DR4	The Jackson Laboratory	Cat#017637
Mouse: OT-II	The Jackson Laboratory	Cat#004194
Mouse: CD45.1	The Jackson Laboratory	Cat#002014
Mouse: OT-II;CD45.1	This paper	N/A
Oligonucleotides		
ill_S-D-Bact-0346-a-S-17: AATGATAC GGCGACCACCGAGATCTACACXXX XXXXXACACTCTTTCCCTACACGACG CTCTTCCGATCTTAGGGRGGCWGC AGTRRGG	Kubinak et al., 2015a	N/A
ill_S-D-Bact-0781-b-A-23: CAA GCAGAAGACGGCATACGAGAT XXXXXXXXGTGACTGGAGTTC AGACGTGTGCTCTTCCGATCTT TCTACHVGGGTATCTAATCCTGTT	Kubinak et al., 2015a	N/A
Prok16SV34_For: AATGATACG GCGACCACCGAGATCTACAC XXXXXXXXACACTCTTTCCCTAC ACGACGCTCTTCCGATCTTGC CTACGGGNBGCASCAG	Takahashi et al., 2014	N/A
Prok16SV34_Rev: CAAGC AGAAGACGGCATACGAGA TXXXXXXXXGTGACTGGAGT TCAGACGTGTGCTCTTCCG ATCTGCGACTACNVGGGTA TCTAATCC	Takahashi et al., 2014	N/A

Author Manuscript Author Manuscript Author Manuscript Author Manuscript

Reagent or resource	Source	Identifier
Software and algorithms		
Biojupies	Torre et al., 2018	https://maayanlab.cloud/biojupies/
USeq		RRID: SCR_004753; http://useq.sourceforge.net/
Novoalign		RRID: SCR_014818; http://www.novocraft.com/
TopHat2	Kim et al., 2013	RRID: SCR_013035; https://ccb.jhu.edu/software/tophat/index.shtml
Limma	Ritchie et al., 2015	RRID: SCR_010943; https://bioconductor.org/
GenomicAlignments	Lawrence et al., 2013	https://bioconductor.org/
QIIME2	Bolyen et al., 2019	RRID: SCR_021258; https://qiime2.org
Cutadapt	Martin, 2011	QIIME2 plugin
VSEARCH	Rognes et al., 2016	QIIME2 plugin
Deblur	Amir et al., 2017	QIIME2 plugin
q2-feature-classifier	Bokulich et al., 2018	QIIME2 plugin
Scikit-learn	Pedregosa et al., 2011	QIIME2 plugin
Seurat	Butler et al., 2018	https://satijalab.org/seurat/
CIPR	Ekiz et al., 2020	https://github.com/atakanekiz/CIPR-Shiny
CellRanger	10X Genomics	https://www.10xgenomics.com/
vegan	Oksanen et al., 2019	RRID: SCR_011950; https://cran.r-project.org/
Change-O	Gupta et al., 2015	https://bitbucket.org/kleinstein/changeo/downloads/
GraphPad Prism	GraphPad Software	RRID: SCR_002798; https://www.graphpad.com:443/
IDEAS Software	Luminex	https://www.luminexcorp.com/imagestreamx-mk-ii/#software
FlowJo	BD Biosciences	https://www.flowjo.com
Other		
2.8 mm ceramic beads	Omni International	Cat#19-646-3
Mini-Beadbeater-16	Biospec Products	Cat#607